Climate Dynamics
https://doi.org/10.1007/s00382-020-05264-9

Analyses of rainfall extremes in East Africa based on observations from rain gauges and climate change simulations by CORDEX RCMs

Charles Onyutha[1]

Received: 5 February 2020 / Accepted: 23 April 2020

Abstract
This study derived twelve Extreme Rainfall Indices (ERIs) such as the Maximum Dry Spell (MDS) and Maximum Wet Spell (MWS) from daily rainfall observed over the period 1961–1990 at nine locations across East Africa. Capacity of six CO-ordinated Regional Climate Downscaling EXperiment (CORDEX) Africa Regional Climate Models (RCMs) driven by twenty six Climate Model Intercomparison Project phase 5 (CMIP5) General Circulation Models (GCMs) to reproduce the observed ERIs with respect to long-term mean and trends was evaluated. Four RCMs and their five driving GCMs were further analyzed with respect to ERIs. Ensemble means of the RCMs' biases in simulating trends in several ERIs were of magnitudes above 50%. On average, biases in reproducing long-term mean were smaller than those for trends in ERIs. The difference between the performances of RCMs and GCMs depended on the selected RCM–GCM pair. The ensemble means of the RCMs reproduced observed ERIs better than the individual RCMs corroborating that the use of multi-model ensembles can boost credibility of climate change simulations and projections. The RCMs performed better than their driving GCMs in reproducing MDS. The biases of both the RCMs and GCMs were smaller in reproducing the MWS than MDS. Nonetheless, in reproducing observed MWS, the ensemble mean of RCMs' biases was slightly larger than that of the driving GCMs indicating possible adding up of the uncertainties from the GCMs and RCMs. Suggested RCMs' improvements regarding aerosol impacts on rainfall include adding missing constituents (like nitrate), and refining the crudely represented components. RCMs also require high resolution description (in both space and time) of land use types, land surface covers and characteristics as well as landscape heterogeneity. The GCMs to be used as the initial and lateral boundary conditions for the RCMs require improvement in their representation of key dynamical and thermodynamical feedbacks in the Tropical Indian Ocean.

Keywords CORDEX RCMs · Climate change · East african rainfall · Trend analysis · Climate change indices · CMIP5 GCMs

1 Introduction

East Africa is familiar with disasters related to both surplus and scarcity of water. Such disasters include rainfall-induced landslides, floods, and droughts. Areas around the Lake Victoria and the Ethiopian Highlands tend to experience high rainfall intensity and, thus, frequent floods and landslides. Some of the rainfall-induced landslides in Bududa district of Uganda occurred in March 2010, March 2011, June 2012, August 2013, October 2018, and December 2019 (ACAPS 2018; Reliefweb 2019). In Ethiopia, several devastating rainfall-induced landslides occurred in Oromia and the Southern Nations Nationalities and People's Region in May 2016 (Floodlist 2016), Koshe garbage dumping area on the outskirt of Addis Ababa in March 2017 (read https://www.bbc.com/news/world-africa-39247381 accessed: 22nd December, 2019), and Konta district of the Southern Ethiopia in September 2019 (Floodlist 2019). These landslides claimed several lives, displaced thousands of local population, and led to several losses of property. On the other hand, increasing temperature, low rainfall total, high

Electronic supplementary material The online version of this article (https://doi.org/10.1007/s00382-020-05264-9) contains supplementary material, which is available to authorized users.

✉ Charles Onyutha
conyutha@kyu.ac.ug

[1] Department of Civil and Building Engineering, Kyambogo University, P.O Box 1, Kyambogo, Kampala, Uganda

Published online: 01 May 2020

evaporation rates, and depleted soil moisture have often led to prolonged droughts in several parts of the East Africa. Between 1950 and 2019, a total of not less than 100 severe drought episodes occurred across East Africa. Over the period 1960–2017, a total of 9, 15, 2, 3, 6, 10, 15, 9, 6, 15, and 10 severe drought episodes occurred in Uganda, Kenya, South Sudan, Eritrea, Burundi, Tanzania, Somalia, Djibouti, Rwanda, Ethiopia, and Sudan, respectively (EM-DAT database EM-DAT (2018) as cited in Haile et al. (2019)). A historically devastating drought across East Africa (especially in Somalia, Djibouti, Ethiopia and Kenya) was that which occurred between July 2011 and the mid-2012. The drought episodes across East Africa between 1960 and 2020 have led to more than 570,000 deaths, and economic losses of at least 1.5 million USD. Due to the anthropogenic forcing, Africa will experience large warming in the twenty-first century (Intergovernmental Panel on Climate Change IPCC 2013). Perhaps, in this line, the widespread 2011 East African drought was linked to climate change (Climate Home News 2013). Generally, during prolonged dry conditions, deaths result mainly from heat-stress, and famine. If no climate change mitigation is implemented, the mortality risk for people aged over 65 years caused by excessive heat stress due to global warming across the middle East and North African region will increase in the distant future to 8–20 times higher than that of the historical period 1951–2005 (Ahmadalipour and Moradkhani 2018). For an effective drought monitoring and management, a systematic framework which can detect drought onset and termination with comprehensive information on how severity, duration, and recovery interrelate during the drought propagation is required. A relevant framework with respect to hydrological drought propagation and recovery considering water quantity and quality can be found provided by Ahmadi and Moradkhani (2019).

To provide an adequate support for climate adaptation with respect to rainfall-related disasters, climate change projections at high spatial and temporal resolution are required at regional and local scales. In this line, Regional Climate Models (RCMs) can be used for analyses of projections of climatic conditions. For the case of East Africa, several RCMs of the CO-ordinated Regional Climate Downscaling EXperiment (CORDEX) Africa are available for evaluation. These RCMs tend to be driven by reanalyses data as the initial and lateral boundary conditions for reproducing observed precipitation, and temperature. Some of these reanalyses or precipitation and temperature products include the Climate Hazards centre Infrared Precipitation with Stations version 2 (CHIRPS2.0) (Funk et al. 2015), Tropical Rainfall Measuring Mission (TRMM) Multi-satellite Precipitation Analysis TMPA 3B42-V7 (Huffman et al 2007), Precipitation Estimation from Remotely Sensed Information using Artificial Neural Networks Climatic Data Record (PERSIANN CDR V1R1) (Ashouri et al. 2015), Princeton Global Forcings (PGF) (Sheffield et al. 2006), and the Africa Rainfall Climatology version 2 (ARC2) (Novella and Thiaw 2013). For the case of East Africa, several studies (Berhane et al. 2020; Harrison et al. 2019; Gebrechorkos et al. 2019; Muthoni et al. 2019; Nashwan and Shahid 2019; Cattani et al. 2018) tended to focus on analyses of long-term trends in reanalyses-based climate indices considering the historical (not future) climatic conditions. Recent studies that assessed capacity of CORDEX in reproducing rainfall over East Africa were Ayugi et al. (2020), Endris et al. (2013), and Kisembe et al. (2018). However, there are a number of gaps from these studies; for instance, they considered reanalysis datasets of monthly scale and did not evaluate CORDEX RCMs with respect to rainfall extremes. Ayugi et al. (2020) assessed the capacity of only one RCM (i.e. RCA4) though downscaled by ten General Circulation Models (GCMs) from phase 5 of the Coupled Model Intercomparison Project (CMIP5). Kisembe et al. (2018) assessed RCMs when driven by ERA-Interim (not GCMs). It is vital that RCMs driven by GCMs (as adopted in this study) can be evaluated for an insight on how the biases of both RCMs and GCMs add up with respect to extreme rainfall conditions. Lack of high quality observed data for evaluation of the RCMs across the entire Africa is a difficult problem (Nikulin et al. 2012). In some of the sub-Saharan countries, even for the cases where weather recording stations are of reasonable number (or density) and distribution, it is very expensive to acquire quality observed climatic data for scientific research. Eventually, reanalyses downscaling simulations can be compared with observed data to assess the performance of the RCMs. However, reanalyses data are normally affected by inhomogeneities from changes over time in the global observing system (Zhang et al. 2011) despite their potential for evaluation of RCMs or to be used for assessment of observed mean climatic conditions. In summary, the dearth of analyses on climate indices under both current and future climatic conditions using station-based weather observations across the East African region was the compelling reason for this study.

Therefore, this is the first study aimed at analyzing Extreme Rainfall Indices (ERIs) based on observed and climate model-based data in the sub-Saharan Africa. To do so, analyses were based on daily rainfall from 9 weather stations across East Africa and simulations from a total of six RCMs driven by twenty six GCMs of the CMIP5 within the framework of CORDEX Africa. From the daily data, a total of twelve ERIs were derived for extreme value analyses, trend detection, and climate impact investigation.

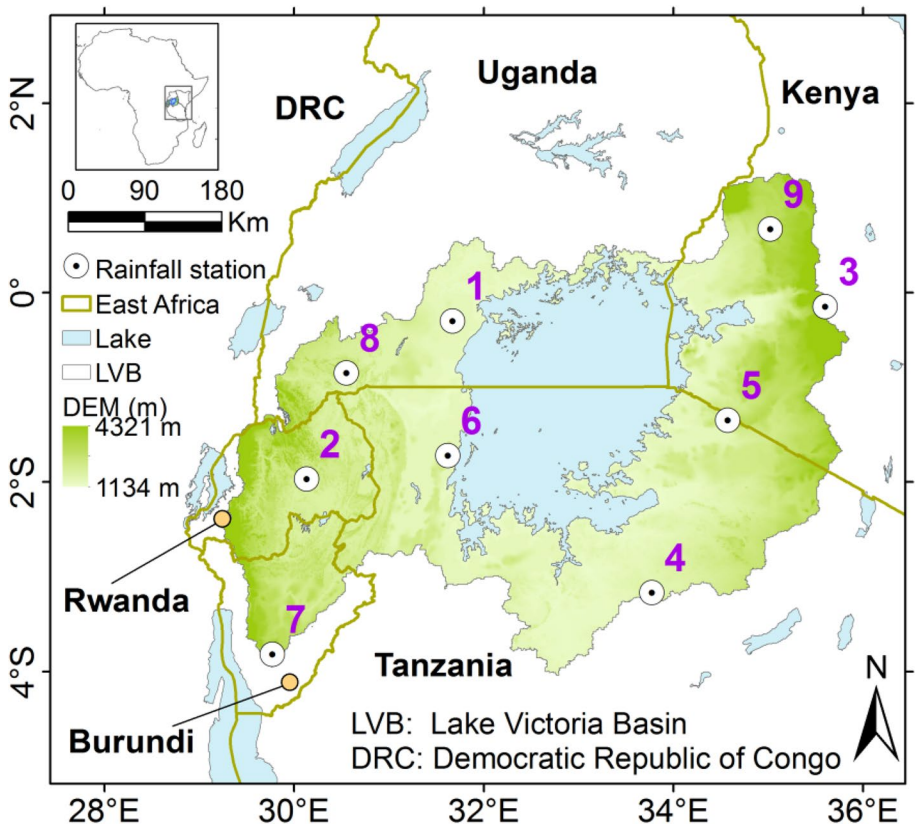

Fig. 1 Study area and location of selected rainfall stations

2 Materials and method

2.1 Study area and rainfall data

The Lake Victoria Basin (LVB, Fig. 1) is located in East Africa and stretches 355 km in the East–West direction (31°37′E to 34°53′E) and 412 km in North–South direction (00°30′ N to 3°12′S). The LVB has a drainage area close to 184,000 km^2 about 37.5% of which comprises the surface of the Lake Victoria. The shoreline of the Lake Victoria is about 4830 km. The LVB stretches into five East African countries including Uganda, Kenya, Tanzania, Rwanda and Burundi (Fig. 1). The background map of the LVB is the Digital Elevation Model (DEM). The hole-filled DEM derived from the USGS/NASA (Jarvis et al. 2008) and processed by the International Centre for Tropical Agriculture (CIAT–CSI–SRTM) using interpolation methods described by Reuter et al. (2007) was downloaded online via the link https://srtm.csi.cgiar.org (accessed: 3rd December, 2019). The elevation ranges from about 1134 m to 4320 m above sea level. The highest point (4321 m) is the peak of Mount Elgon located in the North-eastern part of the LVB. The lowest lying area is the Lake Victoria surface situated at an altitude of 1134 m. The difference between the highest and the lowest point across the LVB is as large as 3186 m.

In this study, focus was given to the LVB for a number of reasons. It is one of the wettest parts of Africa as a continent. Rainfall over this basin controls levels of the Lake Victoria, the largest freshwater body in Africa and world's second largest lake. The LVB experiences both modified equatorial and semi-arid types of climate. Over the lake and its vicinity there is a substantial rainfall which occurs throughout the year (modified equatorial type of climate); however, in some other parts of the LVB even within short distances from the lake shore there is the semi-arid type of climate characterized by intermittent droughts (Anyah et al. 2006; Onyutha and Willems 2015). The rainfall over the LVB is substantially subject to complex influence of topography. The LVB is surrounded by several lakes including Kyoga, Albert, Edward, George, Kivu, Tanganyika, and Turkana. The LVB occupies a depression between the eastern and western rift valleys. Furthermore, to the West, East, North East, South East of the LVB are Mount Rwenzori, Mount Kenya, Mount Elgon, and Mount Kilimanjaro whose peaks are at elevations of 5109 m, 5199 m, 4321, and 5895 m above sea level, respectively. The combined effects of the influences from the Great Lakes (Lake Victoria, Lake Tanganyika, and Lake Malawi) and the high mountains greatly shape the atmospheric dynamics and stability thereby having an important control over the East African regional climate. The above reasons place the LVB as an ideal area to evaluate

climate models in reproducing observed climatology in East Africa, something which is relevant to boost confidence in the climate change projections across the region.

Long-term daily rainfall observed from 9 rain gauges in five countries (Fig. 1) was used for analyses. These rainfall series with temporal coverage over the climate baseline 1961–1990 (as recommended by the World Meteorological Organisation WMO) were obtained from a past study (Onyutha and Willems 2015) in which data quality check and control were performed. Location of each rainfall station can be seen from Fig. 1. An overview of the daily data can be obtained from Table 1 in terms of the long-term (1961–1990) mean and the maximum (Max) rainfall intensity. The long-term mean ranged from 2.5 mm/day (Station 4) to 6.6 mm/day (Station 2). However, values of Max varied from 82.5 mm/day (Station 9) to 129.5 mm/day (Station 4).

2.2 Simulations of CORDEX RCMs

Several RCMS (including CCLM4-8-17, CRCM5, HIRHAM5, RACMO22T, RCA4 and REMO2009) of the CORDEX Africa project (Nikulin et al. 2012) were considered in this study. In CORDEX Africa, the six RCMs made use of twenty six GCMs of the CMIP5 (Table 2) as initial and lateral boundary conditions resulting in simulations for the historical (1950–2005) and future (2006–2100) periods. Based on the CORDEX experiment, the RCMs have a spatial resolution of 0.44 or 50 km resolution with daily temporal scale. Daily future projection series considered in this study were over the periods 2046–2065 (2050s) and 2081–2100 (2090s) under three Representative Concentration Pathways RCP 2.6, RCP 4.5, and 8.5. Also available from the CORDEX framework are the RCMs' evaluation simulation over the period 1990–2008 in which the ERA-Interim reanalyses were used as the initial and lateral conditions to drive the RCMs. As pointed out in Sect. 2.1, the daily observed rainfall was from 1961 to 1990. This meant that the comparison of observed and evaluation simulations of the RCMs could not be possible due to non-overlapping data periods.

2.3 Extreme rainfall Indices (ERIs)

To adequately characterize extreme rainfall conditions, a total of twelve ERIs (Table 3) were calculated from the daily data. Based on the WMO/WCRP/JCOMM ETCCDI recommendations, Zhang et al. (2011) listed 25 climate indices. Ten and fifteen of the twenty five indices from Zhang et al. (2011) are based on precipitation and temperature, respectively. In this study, temperature was not considered for brevity and lack of observed data. Nevertheless, three of the twelve indices derived in this study including the Severe or Maximum Dry Spell (MDS1), Maximum Wet Spell (MWS1), and Rainfall total (TPre1) are respectively analogous to the Consecutive Dry Days (CDD), Consecutive Wet Days (CWD), and Annual total wet-day precipitation (PRCPTOT) of climate change indices listed by Zhang et al. (2011). For in-depth analyses, the ERIs of this study were derived so as to permit extreme value analyses, trend detection, and climate impact investigation. Specifically for extreme value analyses, the Annual Maxima Series (AMS) was extracted in terms of the maximum event from each year. Other ERIs considered were Number of Dry Days (NDD) and Number of Wet Days (NWD).

2.4 Frequency analyses

Frequency of both observed and RCMs-based rainfall extremes was analyzed in terms of return periods (or the recurrence interval between one event and the next, either of equal or larger magnitude). The AMS (see definition from Table 3) was eventually used due to its strong independence of the extreme events. The AMS was sorted from the highest to the lowest. In this way, if h is the sample size of the extracted extreme events or AMS, the largest and the smallest events got ranks of $j = 1$ and $j = h$, respectively. In

Table 1 Overview of selected rainfall stations

No	Station ID	Station name	Mean (mm/day)	Max (mm/day)	Country
1	9,031,026	Kamenyamigo	2.7	90.0	Uganda
2	70,009	Kigali Aero Nyabarongo	6.6	91.9	Rwanda
3	9,035,002	Londiani Forest	3.2	79.7	Kenya
4	9,333,005	Maswa Hydromet	2.5	129.5	Tanzania
5	9,134,008	Nyabassi	3.9	120.0	Tanzania
6	9,131,001	Rubya Mission	3.8	124.8	Tanzania
7	10,161	Ruvyironza	3.6	90.0	Burundi
8	9,030,012	Rwoho Forest	2.6	120.6	Uganda
9	8,935,076	Turbo Forest	3.6	82.5	Kenya

Source: Onyutha and Willems (2015)

Table 2 Overview of CORDEX RCMs' simulations (✓: available, and ×: absent)

RCM	Driving GCM	Historical	RCP2.6	RCP4.5	RCP8.5
REMO2009	MIROC5	✓	✓	×	×
REMO2009	CM5A-LR	✓	✓	×	×
REMO2009	EC-EARTH	✓	✓	✓	✓
REMO2009	GFDL-ESM2G	✓	✓	×	×
REMO2009	HadGEM2-ES	✓	✓	×	×
REMO2009	**MPI-ESM-LR**	✓	✓	✓	✓
CCLM4-8–17	**CNRM-CM5**	✓	✓	✓	✓
CCLM4-8–17	HadGEM2-ES	✓	×	✓	✓
CCLM4-8–17	EC-EARTH	✓	×	✓	✓
CCLM4-8–17	**MPI-ESM-LR**	✓	×	✓	✓
RCA4	EC-EARTH	✓	✓	✓	✓
RCA4	GFDL-ESM2M	✓	×	✓	✓
RCA4	**CanESM2**	✓	×	✓	✓
RCA4	**MPI-ESM-LR**	✓	✓	✓	✓
RCA4	MIROC5	✓	✓	✓	✓
RCA4	**CNRM-CM5**	✓	×	✓	✓
RCA4	NorESM1-M	✓	✓	✓	✓
RCA4	**CSIRO-Mk3-6–0**	✓	✓	✓	✓
RCA4	CM5A-MR	✓	×	✓	✓
RCA4	HadGEM2-ES	✓	✓	✓	✓
RACMO22T	HadGEM2-ES	✓	✓	✓	✓
RACMO22T	EC-EARTH	✓	×	✓	✓
HIRHAM5	EC-EARTH	✓	×	✓	✓
HIRHAM5	NorESM1-M	✓	×	✓	✓
CRCM5	**CanESM2**	✓	×	✓	×
CRCM5	**MPI-ESM-LR**	✓	×	✓	×

RCMs and the driving CMIP5 GCMs whose outputs were considered for comparison are marked bold

the next step, an empirical return period of each event was computed as the ratio of d to j where d is data record length in years (30 years in this case). The sorted AMS was plotted against logarithmic return period. For comparison of the AMS from observed rainfall and historical simulations of the CORDEX RCMs, the Slope of the the Regression lines through Return Periods (SRRP) and the 1-year return level were used.

2.5 Trend analyses

Trend was detected in each rainfall index using the Mann–Kendall MK (Mann 1945; Kendall 1975) test. The values of the standardized MK statistic Z computed using observed rainfall extreme indices were compared with those obtained from the historical simulations of the RCMs.

The MK (Mann 1945; Kendall 1975) test statistic S was computed using:

$$S = \sum_{i=1}^{n-1} \sum_{j=i+1}^{n} \operatorname{sgn}\left(x_j - x_i\right) \tag{1}$$

where x_j and x_i are the sequential data values in a sample of size n, and

$$\operatorname{sgn}\left(x_j - x_i\right) = \begin{cases} 1 & \text{if } \left(x_j - x_i\right) > 0 \\ 0 & \text{if } \left(x_j - x_i\right) = 0 \\ -1 & \text{if } \left(x_j - x_i\right) < 0 \end{cases} \tag{2}$$

For $n \geq 8$, S is approximately normally distributed with the mean $E_S = 0$ and variance V_S given by (Mann 1945; Kendall 1975):

$$V_S = \frac{1}{18}\left(n(n-1)(2n+5) - \sum_{k=1}^{g} t_k(k-1)(2k+5)\right) \tag{3}$$

where: g is the number of tied groups, and t_k is the number of observations in the kth group. The standardized MK test statistic Z which follows the standard normal distribution with mean (variance) of zero (one) was computed using:

$$Z = \begin{cases} \frac{S-1}{\sqrt{V(S)}} & \text{for } S > 0 \\ 0 & \text{for } S = 0 \\ \frac{S+1}{\sqrt{V(S)}} & \text{for } S < 0 \end{cases} \tag{4}$$

Positive and negative values of S indicate positive and negative trends, respectively. The null hypothesis H_0 (no trend) was rejected for $|Z| > Z_{\alpha/2}$ where $Z_{\alpha/2}$ denoted the standard normal variate at the significance level $\alpha\%$; otherwise the H_0 was not rejected at α.

2.6 Performance of the RCMs

RCMs were assessed in terms of how well they reproduced three observed metrics (i) trends in ERIs, (ii) long-term mean of ERIs, and (iii) the frequency of AMS-based extreme events. Performance of the RCMs was assessed in terms of bias, skill score, and Root Mean Squared Error (RMSE).

Table 3 Rainfall indices used in this study

ID	Indicator name	Indicator definition	Unit
AMS	Annual maxima series	Series comprising the maximum rainfall intensity in each year	mm/day
MDS1	Severe dry spell	Annual maximum number of consecutive days with rainfall < 1 mm	days
MDS10	Dry spell	Annual maximum number of consecutive days with rainfall < 10 mm	days
NDD1	Very dry day	Annual number of days each having rainfall < 1 mm	days
NDD5	Dry day	Annual number of days each having rainfall < 5 mm	days
NWD1	Wet day	Annual number of days each having rainfall > 1 mm	days
NWD10	Very wet day	Annual number of days each having rainfall > 10 mm	days
MWS1	Wet spell	Annual maximum number of consecutive days with rainfall > 1 mm	days
MWS5	Very wet spell	Annual maximum number of consecutive days with rainfall > 5 mm	days
TPre1	Rainfall total > 1 mm/day	Annual total rainfall from days with rainfall > 1 mm	mm
TPre5	Rainfall total > 5 mm/day	Annual total rainfall from days with rainfall > 5 mm	mm
TPre10	Rainfall total > 10 mm/day	Annual total rainfall from days with rainfall > 10 mm	mm

2.6.1 Model bias

If A and B are respectively any of the RCM-based and observed ERIs; the RCM bias was computed in terms of the ratio of the $(A-B)$ to B. The best (worst) performing RCM is expected to have the smallest (largest) bias. Graphically, the observed extreme index (see Table 3) was compared with the values computed from the outputs of the RCMs.

2.6.2 Model skill score

Let us consider w as the total number of simulations from the various RCMs. Using the biases at a particular station, the RCMs were ranked in ascending order such that the ranks (C) of 1, 2, …, were respectively given to the first, second,….. best performing models. The worst performing RCM yields $C=w$. The skill score (D_i, %) for the ith simulation can be computed using.

$$D_i = \left(1 - \frac{C_i}{w}\right) \times 100 \quad for\, 1 \le i \le w \tag{5}$$

The skill scores of the RCMs were computed based on how well they reproduced observed ERIs at only one rainfall station. This was repeated such that how one RCM performed at all the rainfall stations was noted. In the next step, for a particular metric, for instance, trend in rainfall indices, the mean of the skill scores of each RCM across all the rainfall stations was obtained and denoted as MSC. Here, the best performing RCM considering the entire study area would have the highest value of MSC.

With respect to frequency analyses, the MSC was obtained by averaging results of Eq. (5) applied to 1-year quantile, and the SRRP (see Sect. 2.4).

2.6.3 Co-variation of observed and RCMs-based extreme indices

To assess the co-variation of the observed and RCMs-based extreme indices, the coefficient of determination (R^2) was computed using

$$R^2 = \frac{\left(\sum_{i=1}^{n}\left(A_i - A^m\right)\left(B_i - B^m\right)\right)^2}{\sum_{i=1}^{n}\left(A_i - A^m\right)^2 \sum_{i=1}^{n}\left(B_i - B^m\right)^2} \tag{6}$$

where A and B are as already defined in Sect. 2.6.1 while A^m and B^m denote the mean value of A's and B's, respectively. The best and worst RCM can be given by R^2 equal to 1 and 0, respectively.

2.6.4 Root mean squared error (RMSE)

In frequency analyses, the AMS is sorted in descending order to get the return periods. In this case, correlation between observed and RCM-based quantiles would always be equal to 1 thereby making it unsuitable to use R^2. Therefore, the differences between observed and RCMs-based rainfall quantiles were computed in terms of the RMSE using

$$RMSE = \sqrt{\frac{1}{n}\sum_{i=1}^{n}\left(A_i - B_i\right)^2} \tag{7}$$

For evaluating the mismatch between the observed and RCMs-based rainfall indices (in their unsorted form), the RMSE was divided by B^m to obtain RRM (Ratio of RMSE to mean), a metric without unit and its order of magnitude reduced compared with the RMSE. Like the RMSE, the best performing model also has RRM equal to zero.

2.7 Comparison of RCMs and their corresponding driving GCMs

Nine simulations of RCMs and the driving CMIP5 GCMs (marked bold in Table 2) were compared through Eq. (7) applied to AMS, MDS1, MDS10, MWS1, MWS5, and rainfall quantiles. This was to understand the influence of the GCMs as the initial and lateral boundary conditions on performance of the RCMs in reproducing observed extreme rainfall conditions across the study area.

2.8 Impacts of climate change

Impacts of climate change was obtained by comparing extreme rainfall indices (see Table 3) from observed and RCMs-based projected rainfall over the 2050s and 2090s. With respect to frequency of extreme rainfall quantiles, the impact of climate change was obtained in terms of the ratio of the difference between the future and observed extreme rainfall to the observed rainfall with the corresponding return period. In other words, a selected rainfall event from the baseline period 1960–1991 was compared with the future quantile of the corresponding return period.

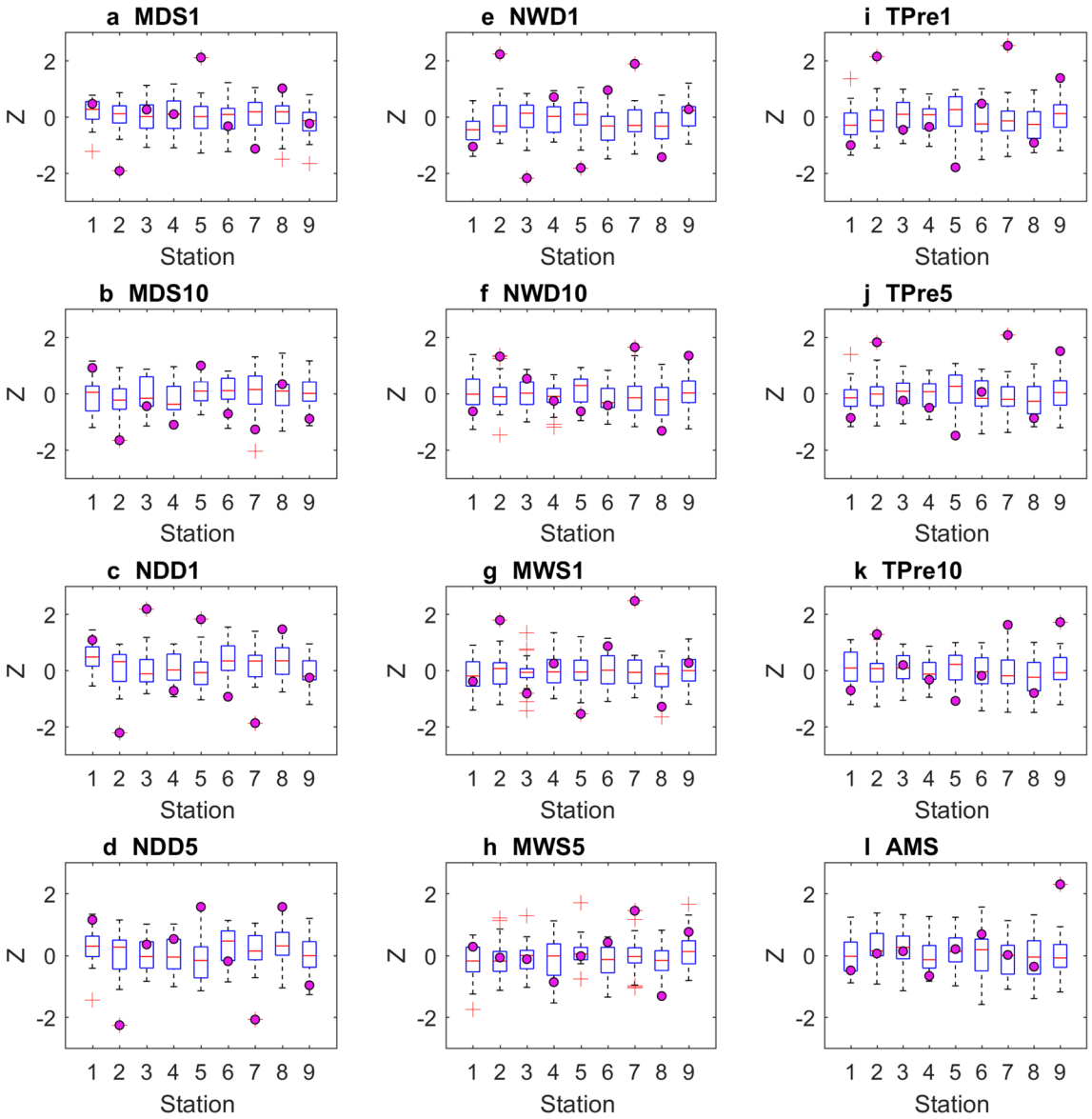

Fig. 2 Comparison of trends in (**a**) MDS1, (**b**) MDS10, (**c**) NDD1, (**d**) NDD5, (**e**) NWD1, (**f**) NWD10, (**g**) MWS1, (**h**) MWS5, (**i**) TPre1, (**j**) TPre5, (**k**) TPre10, (**l**) AMS from observed rainfall and series obtained from historical simulations of RCMs. The filled-in marker in each chart denotes the value obtained using observed rainfall at a particular station

3 Results

3.1 Performance of RCMs regarding trends and long-term mean of each rainfall index

Figure 2 shows values of trend statistic Z for the extreme rainfall indices (see Table 3) over the climate baseline (1961–1990). The simulations of the RCMs were characterized by over-estimation or under-estimation of the trends in observed rainfall indices (Fig. 2a–l). The rainfall extreme index for which the RCMs yielded the best performance at almost all the selected rainfall stations was the AMS (Fig. 2l). Even for the AMS, all the RCMs underestimated the observed trend at Station 9. The ensemble means of the RCMs' biases were large (all above absolute value of 50%) for several metrics MDS10, NDD1, NDD5, NWD1, NWD10, TPre1, TPre5, and TPre10 (Fig. 2b–f, i–k). This means that even by considering averaged trends from the RCMs, the wet and dry conditions across the study area remained poorly reproduced by the CORDEX simulations. Nevertheless, the minimum values from the ensemble means of RCMs' biases for AMS, MDS1, MWS1, and MWS5 were − 20.2%, − 19.0%,− 48.4%, and

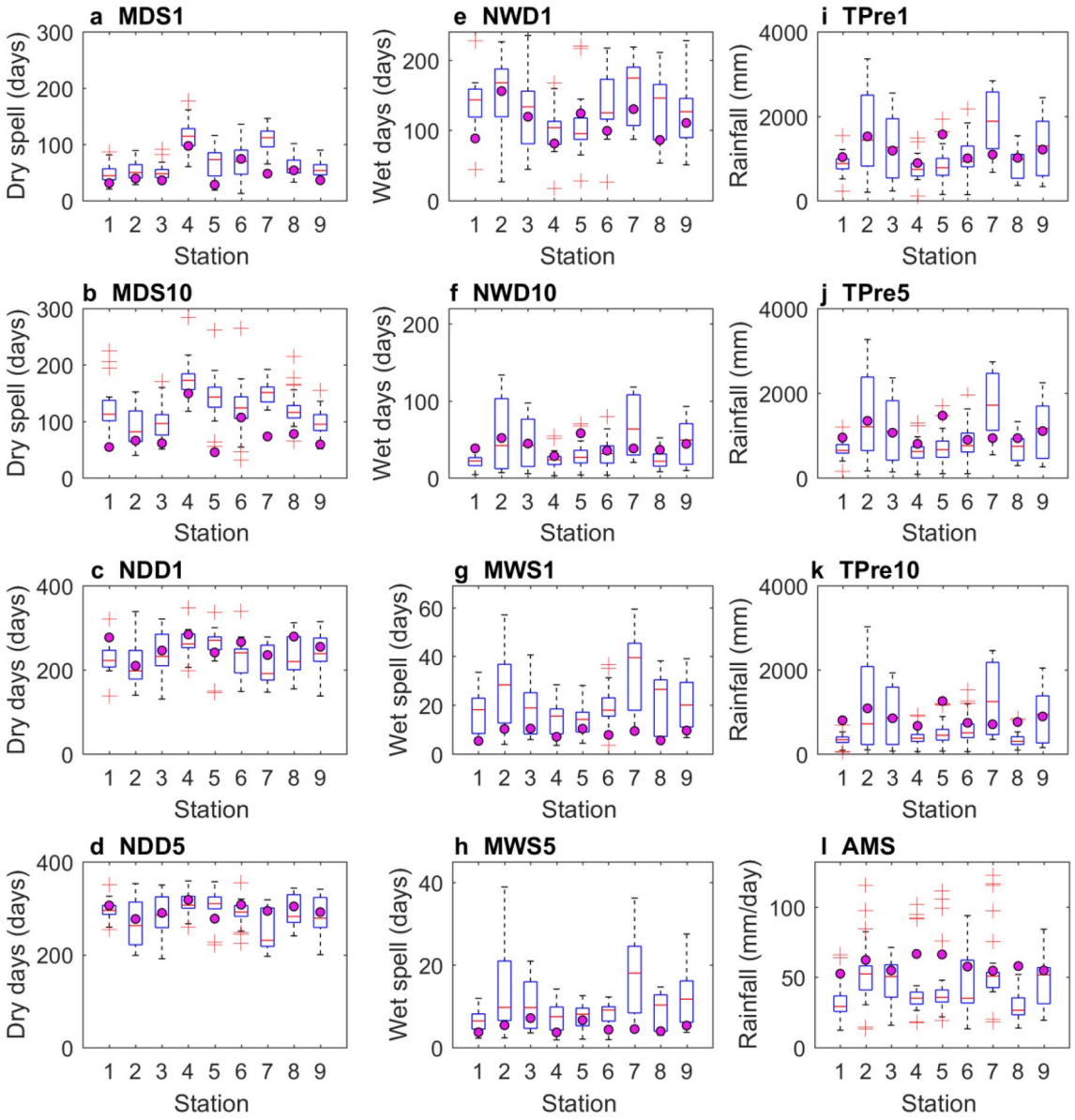

Fig. 3 Long-term (1961–19,901) mean of (**a**) MDS1, (**b**) MDS10, (**c**) NDD1, (**d**) NDD5, (**e**) NWD1, (**f**) NWD10, (**g**) MWS1, (**h**) MWS5, (**i**) TPre1, (**j**) TPre5, (**k**) TPre10, (**l**) AMS from observed rainfall and series obtained from historical simulations of the RCMs. The filled-in marker in each chart denotes the value obtained using observed rainfall at a particular station

− 3.7% at Stations 5, 9, 1 and 3, respectively. On a cursory look at the box plots, the range of the trend statistic *Z* varied from one station to another. This indicates that the difference among the RCMs in capturing trends in the rainfall indices depended on the site to site variability in rainfall extremes across the study area.

Figure 3 shows comparison of long-term mean of rainfall indices based on observed and RCMs' historical simulations. At the various stations, the RCMs exhibited, to varying extents, under-estimations and over-estimations of the observed long-term mean of rainfall indices (Fig. 3a–l). Most RCMs over-estimated MWS1, MSW5, MDS1 and MDS10 (Fig. 3a–b, g–h). However, most RCMs under-estimated AMS (Fig. 3l). Considering the entire LVB, the best performance of the RCMs was for the NDD5, followed by NDD1 and AMS. Across the study area, the range (minimum, maximum) of the ensemble mean of RCMs' biases for NDD5, NDD1 and AMS was (− 15.2%, 10.0%), (− 17.8%, 7.4%) and (− 48.8%, 4.1%), respectively. Biases were generally large (above 100%) in MDS1 (Stations 5 and 7), MDS10 (stations 1, 5, and 7), MWS1 (Stations 1–2, and 6–9), and MWS5 (Stations 2, and 6–9). Increasing threshold from 1 to 5 mm led to an increase in the number of dry days in each year (Fig. 3c–d). Similarly, the length of dry spell was higher for threshold of 10 mm than 1 mm (Fig. 3a–b). However, increasing the rainfall threshold led to a decrease in the number of wet days (Fig. 3e–f), and the rainfall totals (Fig. 3i–k). The RCMs exhibited considerable bias in capturing the changes in observed ERIs as a result of increasing the threshold from 1 to 5 mm or 10 mm.

Figure 4 shows performance of the RCMs with respect to trends and long-term mean of ERIs. Figure 4 comprises results for further analyses related to the biases already presented in terms of trends (Fig. 2) and long-term mean (Fig. 3) of the ERIs. Figures 2 and 3 which simply indicated how the RCMs' values of each metric such as the AMS were close to the observed one. At this point of analysis, it still remained unclear which RCMs exhibited poor or top performance. Eventually, results summarized in Fig. 4 are based on the mean of the skill scores (MSC based on Eq. 4) of a particular RCM obtained at all the selected rainfall stations. The details of the skill scores for each RCM simulation at the various stations can be found in Tables S2-S13 of the Supplementary Material M1. In most cases, there was no RCM that performed best for a particular rainfall index at all the rainfall stations considering both trends and long-term mean (Fig. 4a–b). However, RCA4_HadGEM2-ES was the best in simulation of observed NDD1, NDD5, and NWD1 across the entire study area (Fig. 4a, Tables S5–S7 of the Supplementary Material M1). Top performance in simulation of observed trends at NDD5, NWD10, MWS5, TPre1, TPre5, and TPre10 (Fig. 4b) was exhibited by CRCM5_MPI-ESM-LR. Considering the entire LVB, RCA4_MIROC5 registered top performance regarding trends in AMS, NDD1, NWD1, MWS1, and TPre1 (Fig. 4b). The first five performing RCMs for reproducing the long-term mean of the ERIs across the entire study area were HIRHAM5_EC-EARTH, RCA4_NorESM1-M, RCA4_MPI-ESM-LR, CCLM4-8-17_MPI-ESM-LR, and RCA4_CM5A-MR (Fig. 4a). Similarly, with respect to trends in ERIs, the top five RCMs were CRCM5_MPI-ESM-LR, RCA4_MPI-ESM-LR, RCA4_CanESM2, CRCM5_CanESM2, and RCA4_CSIRO-Mk3-6-0 (Fig. 4b).

Figure 5 shows measures of the differences between the RCM-based and observed ERIs in terms of RRM. It is vital to note that the smaller the RRM value the better the performance of a selected RCM. Like in Fig. 3, the best performance of the RCMs was generally for NDD5 and NDD1 (Fig. 5c–d). RMM for NWD1 and NWD10 (Fig. 5e–f) was also low for some models. Large values of RRM were obtained at some stations for the maximum dry spells (Fig. 5a–b), and wet spells (Fig. 5 g–h). Considering Station 7, it can be seen that increasing threshold from 1 to 10 mm led to an increase in the RRM (Fig. 5i–k). These results indicate the difficulty in reproducing observed dry and wet spells among other indices. The detailed performance for each RCM at a particular station can be found in Tables T1-T12 of the Supplementary Material M2. For instance, the best performance (in terms of the lowest RRM) for AMS at Stations 4–5 and 8 was by CRCM5_CanESM2. At Station 7, the lowest RRM (0.38) was obtained by five RCMs including RCA4_CanESM2, RCA4_CM5A-MR, RCA4_CSIRO-Mk3-6–0, RCA4_MIROC5, and RCA4_NorESM1-M. The lowest RRM values at Stations 1–3, and 6 were 0.39, 0.30, 0.32, 0.38, 0.29, obtained by REMO2009_MIROC5, RCA4_GFDL-ESM2M, RCA4_EC-EARTH, REMO2009_HadGEM2-ES, and RCA4_CM5A-MR, respectively. By considering the average of the RRM values for each RCM at all the selected stations, the best performance (RRM = 0.44) was obtained by CRCM5_CanESM2. For other rainfall indices considering performance of RCMs at all the rainfall stations, the lowest RRM for MDS1mm, MDS10mm, NDD1mm, NWD10mm, NWD1mm, NDD5mm, MWS1mm (or MWS5mm), TPre1mm (or TPre5mm), and TPre10mm was obtained by CRCM5_MPI-ESM-LR,CRCM5_MPI-ESM-LR, RCA4_HadGEM2-ES,CCLM4-8-17_CNRM-CM5, RCA4_HadGEM2-ES, RCA4_HadGEM2-ES, REMO2009_MPI-ESM-LR, RACMO22T_EC-EARTH, and CCLM4-8-17_CNRM-CM5, respectively.

Figure 6 shows strength of the co-variation of observed and RCMs-based rainfall indices. Like for RRM, the details of how the RCMs yielded values plotted in Fig. 6a–l can be found in Tables T1-T12 of the Supplementary Material M2. For instance, the maximum R-squared values for reproducing the variation in AMS and MDS1 were 32.8%,

(a) *MSC* based on mean	AMS	MDS1	MDS10	NDD1	NDD5	NWD1	NWD10	MWS1	MWS5	TPre1	TPre5	TPre10	Overall
CCLM4-8-17_EC-EARTH	54.3	42.7	35.5	42.3	69.7	42.3	62.4	17.1	45.7	69.2	65.4	63.2	50.8
CCLM4-8-17_HadGEM2-ES	59.8	18.4	9.0	63.2	42.7	63.2	35.9	65.4	74.4	41.0	39.3	48.3	46.7
CCLM4-8-17_MPI-ESM-LR	33.3	39.3	34.6	54.3	64.5	54.3	62.4	46.6	64.5	66.7	70.5	73.9	55.4
CRCM5_CanESM2	66.7	69.7	73.9	35.0	41.0	35.0	41.9	50.4	49.6	36.3	38.9	54.3	49.4
CRCM5_MPI-ESM-LR	57.3	67.9	81.6	26.9	29.1	26.9	49.6	41.5	42.7	44.4	49.6	70.5	49.0
HIRHAM5_EC-EARTH	62.8	68.8	65.0	58.5	59.4	58.5	49.6	69.2	74.4	42.7	42.3	48.3	58.3
HIRHAM5_NorESM1-M	34.6	20.9	14.1	54.3	41.5	54.3	39.7	74.4	70.1	37.2	37.2	39.3	43.1
RACMO22T_EC-EARTH	5.6	59.4	31.2	31.6	43.2	31.6	52.6	15.0	35.5	64.1	62.4	47.4	40.0
RACMO22T_HadGEM2-ES	3.0	48.7	20.9	40.6	49.6	40.6	33.3	35.5	52.1	46.2	41.5	22.6	36.2
RCA4_CanESM2	52.1	34.2	59.0	50.4	36.3	50.4	48.7	28.2	14.5	52.6	49.6	45.3	43.4
RCA4_CM5A-MR	62.4	64.1	74.4	44.4	36.3	44.4	56.0	38.0	28.6	58.5	57.7	51.7	51.4
RCA4_CNRM-CM5	49.1	59.8	63.2	52.1	52.1	52.1	53.8	29.9	24.8	61.1	56.4	50.9	50.5
RCA4_CSIRO-Mk3-6-0	45.7	38.9	38.5	47.0	46.2	47.0	40.6	32.1	25.6	49.6	45.7	33.8	40.9
RCA4_EC-EARTH	68.8	56.0	78.6	40.2	28.6	40.2	48.3	18.8	11.1	40.6	46.2	48.7	43.8
RCA4_GFDL-ESM2M	62.8	59.8	64.5	42.7	43.6	42.7	47.9	19.2	9.4	54.3	47.0	38.9	44.4
RCA4_HadGEM2-ES	38.0	30.8	31.2	72.2	75.6	72.2	52.6	60.3	47.9	50.9	50.0	49.6	52.6
RCA4_MIROC5	49.1	26.5	41.0	50.0	48.7	50.0	53.4	40.2	35.9	55.1	56.4	43.2	45.8
RCA4_MPI-ESM-LR	61.1	39.7	64.5	55.1	47.0	55.1	62.8	34.6	19.2	65.0	67.1	58.5	52.5
RCA4_NorESM1-M	51.3	44.4	43.6	57.3	62.4	57.3	56.8	45.3	45.3	63.7	57.7	53.0	53.2
REMO2009_CM5A-LR	44.9	40.6	21.8	41.0	39.3	41.0	30.3	76.9	67.1	24.4	24.4	32.5	40.3
REMO2009_EC-EARTH	40.2	50.0	50.9	71.4	53.0	71.4	35.0	84.2	82.1	32.5	32.1	32.1	52.9
REMO2009_GFDL-ESM2G	60.7	44.9	44.4	53.8	53.0	53.8	40.2	77.8	72.2	35.9	37.2	42.3	51.4
REMO2009_HadGEM2-ES	44.0	39.3	39.7	39.7	39.3	39.7	30.3	76.9	64.1	25.2	26.5	30.8	41.3
REMO2009_MIROC5	50.4	60.3	52.1	49.6	50.4	49.6	47.9	76.1	68.8	41.9	42.7	49.1	53.2
REMO2009_MPI-ESM-LR	50.0	60.3	55.1	56.4	54.3	56.4	41.9	78.6	79.5	34.6	35.9	41.5	53.7
CCLM4-8-17_CNRM-CM5	41.9	65.0	62.0	19.7	43.6	19.7	77.8	20.5	50.4	56.4	70.5	80.3	50.6

(b) *MSC* for trend *Z*	AMS	MDS1	MDS10	NDD1	NDD5	NWD1	NWD10	MWS1	MWS5	TPre1	TPre5	TPre10	Overall
CCLM4-8-17_EC-EARTH	39.3	39.3	49.1	44.0	47.0	43.6	38.9	40.2	50.0	41.0	41.0	38.5	42.7
CCLM4-8-17_HadGEM2-ES	48.7	57.7	66.7	56.0	46.2	55.6	41.9	35.0	7.7	51.3	52.6	54.3	47.8
CCLM4-8-17_MPI-ESM-LR	47.0	45.7	35.5	53.4	53.8	53.4	50.4	50.4	26.9	42.7	43.2	34.6	44.8
CRCM5_CanESM2	50.9	46.6	58.1	52.6	60.3	52.6	50.9	40.2	0.0	51.3	57.7	50.9	47.6
CRCM5_MPI-ESM-LR	50.9	51.3	55.6	54.3	68.4	53.0	63.7	41.5	57.7	60.7	65.0	65.8	57.3
HIRHAM5_EC-EARTH	36.8	36.8	55.1	56.8	52.6	58.1	39.7	50.0	15.4	42.3	44.0	37.6	43.8
HIRHAM5_NorESM1-M	29.5	35.0	47.0	42.7	50.0	42.7	39.7	46.2	3.8	48.7	48.7	41.9	39.7
CCLM4-8-17_CNRM-CM5	51.7	62.0	32.9	30.3	47.4	30.8	55.6	49.1	23.1	54.3	54.3	55.6	45.6
RACMO22T_EC-EARTH	53.4	50.0	42.7	47.0	62.4	46.6	49.6	51.7	34.6	56.0	56.8	53.8	50.4
RACMO22T_HadGEM2-ES	51.3	63.7	57.7	47.9	43.6	49.1	62.0	46.6	84.6	50.4	50.0	57.7	55.4
RCA4_CanESM2	46.6	52.6	54.3	42.3	37.6	41.0	41.0	45.3	92.3	38.5	29.9	33.8	46.3
RCA4_CM5A-MR	44.0	42.3	44.9	57.7	59.4	58.1	43.2	42.3	53.8	52.6	53.8	50.0	50.2
RCA4_CNRM-CM5	62.4	57.3	30.3	51.3	48.3	50.4	59.0	44.4	88.5	49.1	51.3	56.8	54.1
RCA4_CSIRO-Mk3-6-0	39.3	48.7	37.6	38.5	48.7	38.9	38.0	41.0	42.3	45.3	48.3	40.6	42.3
RCA4_EC-EARTH	38.5	48.3	51.7	42.7	43.6	42.7	42.7	53.4	61.5	44.9	40.2	44.4	46.2
RCA4_GFDL-ESM2M	53.0	17.5	49.6	43.2	44.0	43.2	51.7	47.9	65.4	48.3	41.5	47.0	46.0
RCA4_HadGEM2-ES	48.3	49.6	40.6	55.1	37.6	54.3	45.3	55.6	73.1	32.9	36.8	44.0	47.8
RCA4_MIROC5	57.7	53.0	50.4	62.8	46.2	62.8	60.3	63.2	30.8	56.4	54.7	56.0	54.5
RCA4_MPI-ESM-LR	32.5	32.1	43.2	34.6	30.3	34.6	32.5	53.0	96.2	35.9	36.8	33.8	41.3
RCA4_NorESM1-M	55.1	56.8	50.0	54.3	48.7	53.8	41.0	41.5	38.5	44.9	40.2	46.6	47.6
REMO2009_CM5A-LR	49.1	40.2	47.4	48.7	40.2	50.0	54.7	56.0	46.2	43.6	44.0	55.6	48.0
REMO2009_EC-EARTH	67.5	64.1	46.6	48.7	48.7	47.9	28.6	54.7	11.5	48.3	49.1	39.3	46.3
REMO2009_GFDL-ESM2G	43.6	45.3	36.8	47.0	58.5	47.9	67.5	51.3	76.9	67.9	71.4	61.5	56.3
REMO2009_HadGEM2-ES	56.0	53.8	65.4	42.3	41.5	41.9	50.4	57.3	80.8	49.1	44.0	50.4	52.7
REMO2009_MIROC5	41.0	34.6	46.6	61.5	47.4	61.1	49.6	49.1	19.2	54.3	50.4	49.1	47.0
REMO2009_MPI-ESM-LR	56.0	65.8	54.3	34.2	37.6	35.9	52.1	43.2	69.2	39.3	44.4	50.4	48.5

◂**Fig. 4** Mean of Skill Scores (MSC) of RCMs for (**a**) long-term mean, and (**b**) trends in rainfall indices. In the last column, "Overall" was obtained by averaging skill scores in columns (2)–(13)

and 24.6% all obtained at Station 4 by HIRHAM5_EC-EARTH. The maximum amounts of variance that could be explained in NWD10mm (22.89%), NDD5mm (23.67%), TPre1mm (25.56%), and TPre10mm (24.84%) were all obtained at station 8 and more over by REMO2009_EC-EARTH. The largest R-squared for MWS5mm (24.96%), MDS10mm (30.25%), MWS1mm (23.12%), and TPre10mm (23.16%) were obtained by CCLM4-8-17_EC-EARTH, RCA4_NorESM1-M, RACMO22T_EC-EARTH, and HIR-HAM5_EC-EARTH at stations 1, 3, 6, and 7, respectively. Furthermore, the highest R-squared values for NDD1mm (33.92%) and NWD1mm (33.96%) were all obtained at station 6 by one RCM i.e. REMO2009_EC-EARTH. Furthermore, the average of the R-squared values for each RCM across all the rainfall stations was less than 10%. This indicated the reduced capacity of the RCMs to reproduce spatial and temporal variation in rainfall indices across the study area.

3.2 Performance of RCMs in reproducing frequency of observed rainfall extremes

Figure 7 shows comparison of the frequency of observed and RCMs-based extreme rainfall events. Most quantiles

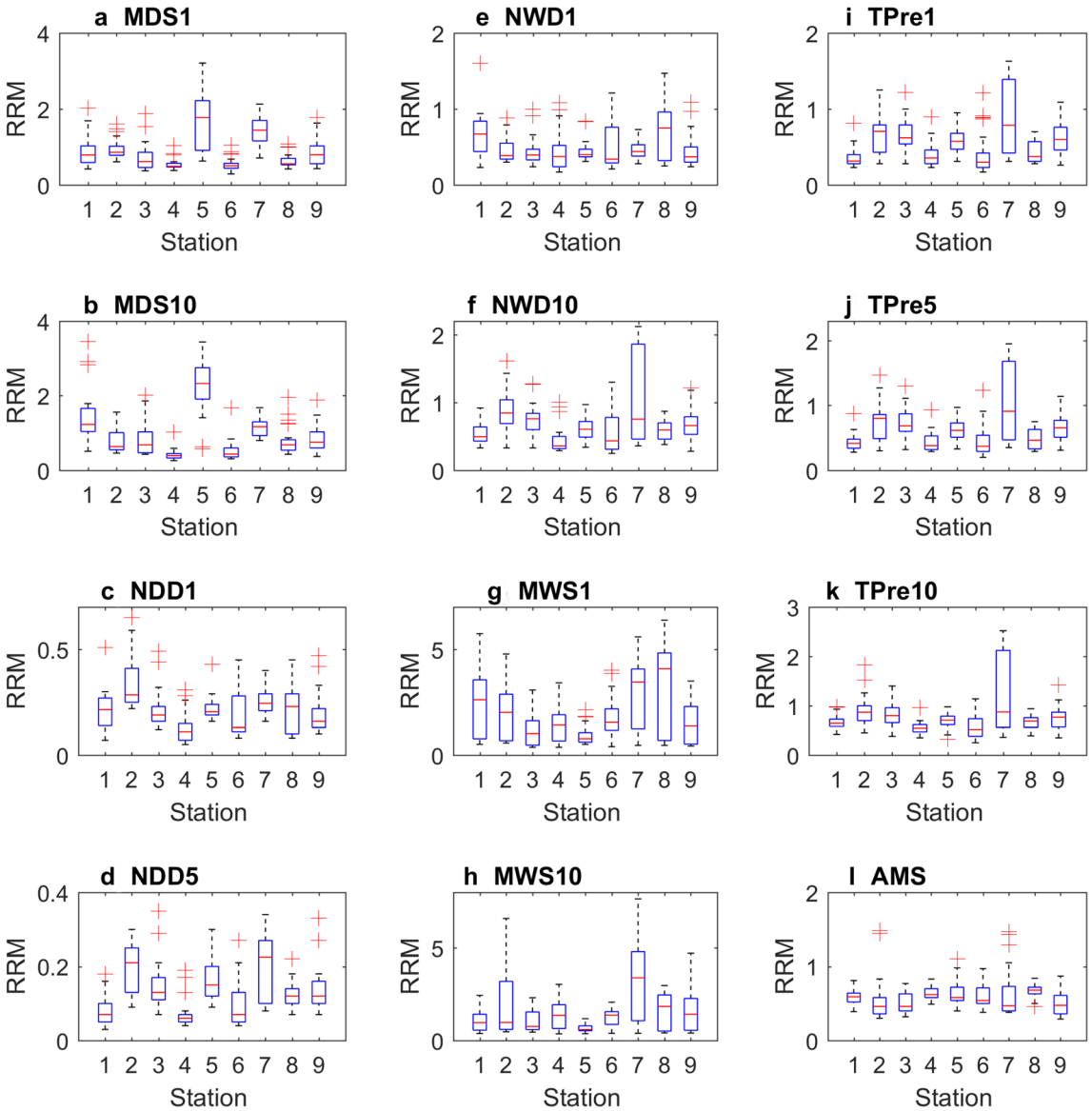

Fig. 5 RMM based on (**a**) MDS1, (**b**) MDS10,(**c**) NDD1, (**d**) NDD5, (**e**) NWD1, (**f**) NWD10, (**g**) MWS1, (**h**) MWS5, (**i**) TPre1, (**j**) TPre5, (**k**) TPre10, (**l**) AMS from observed rainfall and series obtained from historical simulations of the RCMs

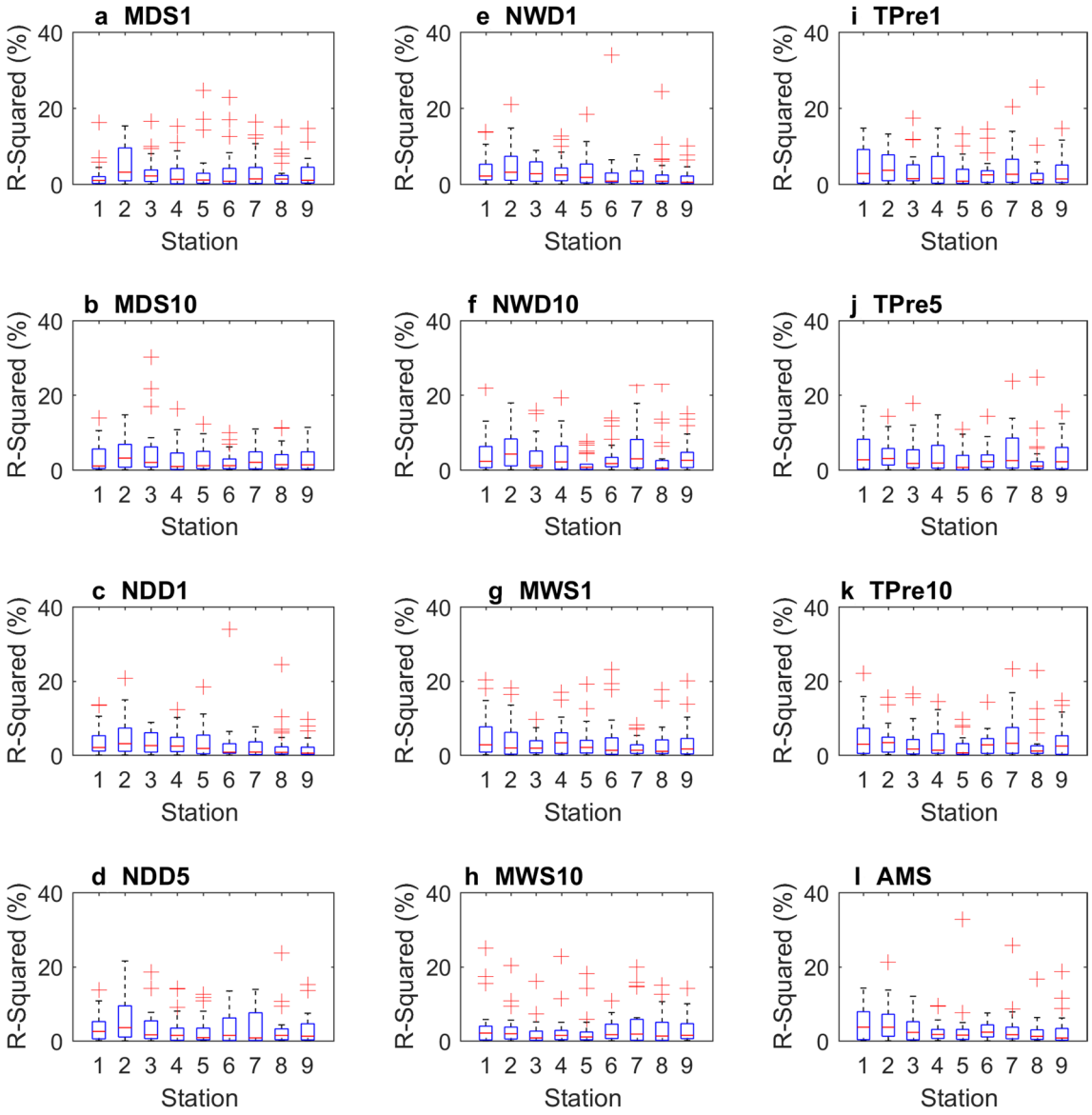

Fig. 6 R-squared based on (**a**) MDS1, (**b**) MDS10, (**c**) NDD1, (**d**) NDD5, (**e**) NWD1, (**f**) NWD10, (**g**) MWS1, (**h**) MWS5, (**i**) TPre1, (**j**) TPre5, (**k**) TPre10, (**l**) AMS from observed rainfall and series obtained from historical simulations of the RCMs

from the RCMs fell below those for the observed rainfall extremes (Fig. 7a–i). Nevertheless, the observed quantiles fell within the ranges of the outputs from the RCMs. This showed good performance of the RCMs when considered collectively. However, the outputs of RCM named CCLM4-8-17 driven by the GCMs EC-EARTH, MPI-ESM-LR, and CNRM-CM5 tended to over-estimate rainfall quantiles at most of the selected locations or stations. At Station 8 (and Station 1 to some extent), the observed quantiles were under-estimated by the outputs of almost all the RCMs (Fig. 5a, h). Considering the entire range of return periods 1–30 years plotted in Fig. 7, the RMSE of each RCM computed on quantiles can be seen summarized in Table 4. The ensemble mean of the RCMS for reproducing quantiles over the range of return periods 1–30 years was 24.5, 25.6, 16.5, 34.3, 34.6, 26.4, 22.9, 30.4, and 17.7 mm/day at Stations 1 to 9, respectively. The worst performance at Stations 1, 3, 6, 8, and 9 was all obtained by RACMO22T_HadGEM2-ES in terms of RMSE 42.1, 41.3, 46.2, 46.4, and 37.5 mm/day, respectively. The maximum RMSE at Stations 2 and 5 was 80.7, and 57.6 mm/day all obtained by CCLM4-8-17_MPI-ESM-LR. The worst performance at Stations 4 and 7 was 50.4 and 69.5 mm/day obtained by RACMO22T_EC-EARTH, and CCLM4-8-17_CNRM-CM5, respectively.

Figure 7 can be understood using the concept of extreme value analyses. In case such plots as in Fig. 7 are made using peaks-over-threshold, the extreme events would follow the

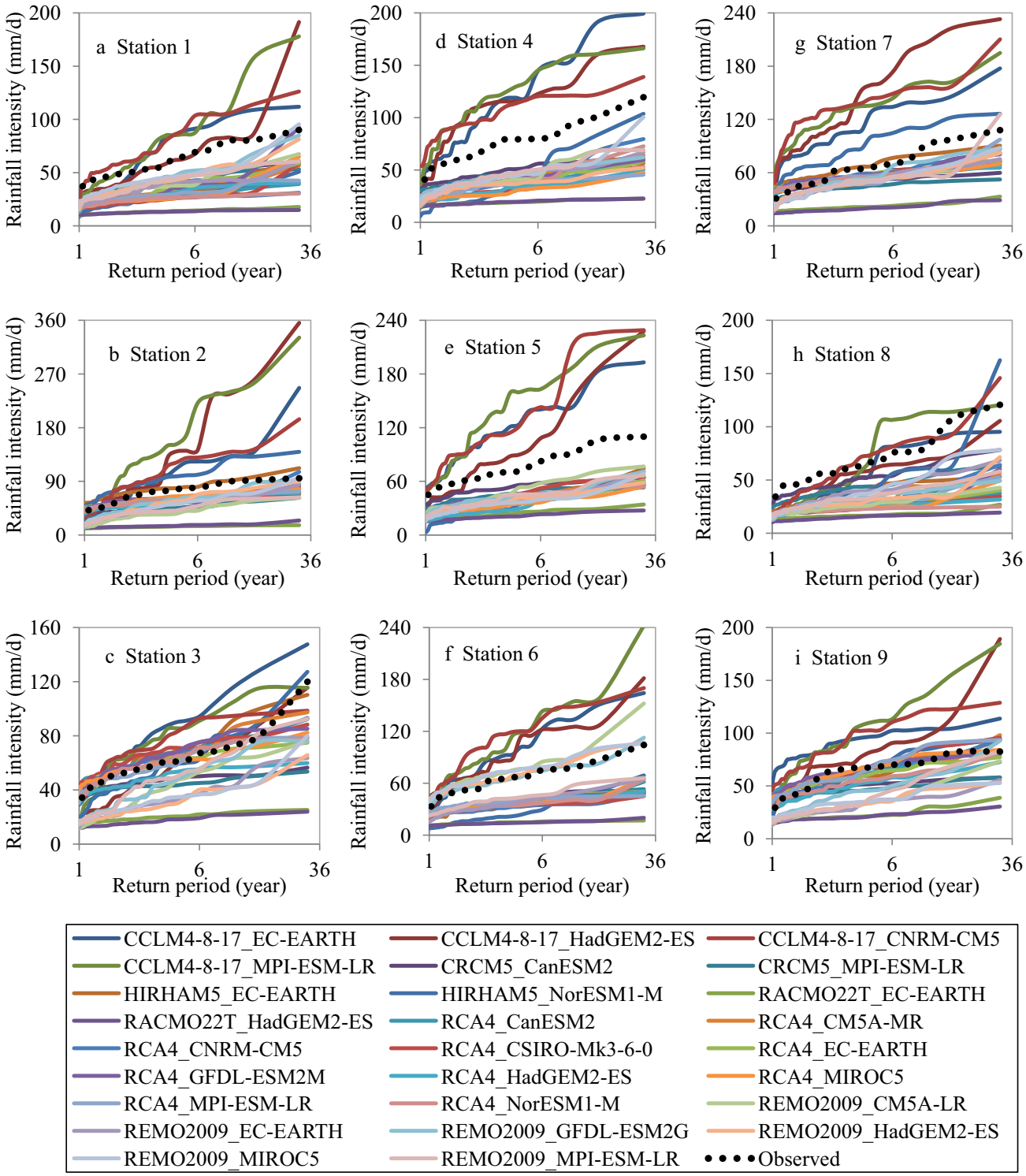

Fig. 7 Quantile–quantile plot of observed and RCMs-based extreme rainfall at (**a**)–(**i**) Stations 1–9. All the charts share the same legend

Generalized Pareto Distribution (GPD) of Pickands (1975). However, the AMS used in Fig. 7 is well known to follow the Generalised Extreme Value (GEV) distribution of Jenkinson (1955). Following some asymptotic sense, the linearity of the tail of the distribution characterizing the observed extreme events is normally associated with the Gumbel distribution (Gumbel 1958) of the GEV or the exponential case of the GPD. Nevertheless, such linearity for the

Table 4 RMSE (mm/d) of CORDEX RCMs on frequency of quantiles

Model	Station								
	1	2	3	4	5	6	7	8	9
CCLM4-8-17_EC-EARTH	17.8	35.0	20.5	36.3	39.6	28.8	44.0	18.0	29.6
CCLM4-8-17_HadGEM2-ES	19.8	72.3	14.0	32.7	31.2	27.1	69.2	18.2	23.0
CCLM4-8-17_MPI-ESM-LR	25.4	80.7	16.7	40.4	57.6	44.2	62.0	20.4	36.5
CRCM5_CanESM2	18.6	17.7	16.0	24.2	19.8	23.4	16.3	14.3	12.9
CRCM5_MPI-ESM-LR	18.3	24.1	18.1	27.5	26.3	23.2	20.1	21.4	15.4
HIRHAM5_EC-EARTH	25.3	10.4	7.0	30.9	27.8	29.4	9.8	26.3	6.1
HIRHAM5_NorESM1-M	30.5	21.7	9.5	38.9	41.5	37.4	21.7	26.3	7.7
CCLM4-8-17_CNRM-CM5	17.1	32.6	14.4	29.3	50.6	42.0	69.5	13.1	28.1
RACMO22T_EC-EARTH	41.7	51.4	38.9	50.4	45.4	46.1	38.4	44.5	36.3
RACMO22T_HadGEM2-ES	42.1	49.9	41.3	50.3	47.9	46.2	40.1	46.4	37.5
RCA4_CanESM2	28.3	13.6	7.7	34.8	33.0	24.5	14.2	36.4	7.4
RCA4_CM5A-MR	24.3	12.2	6.9	32.2	31.0	26.5	11.3	32.7	6.0
RCA4_CNRM-CM5	31.9	14.4	6.4	33.3	33.1	30.0	11.1	34.9	6.5
RCA4_CSIRO-Mk3-6–0	30.7	13.6	9.9	39.4	29.1	28.9	12.2	38.4	7.0
RCA4_EC-EARTH	23.6	12.4	9.3	32.2	30.8	24.5	12.4	36.2	6.7
RCA4_GFDL-ESM2M	24.8	9.8	8.5	32.7	29.6	25.3	11.2	34.3	6.9
RCA4_HadGEM2-ES	27.8	15.4	14.2	40.0	39.3	25.0	13.6	38.2	12.0
RCA4_MIROC5	27.8	9.8	7.9	41.2	36.4	25.5	13.5	37.2	5.0
RCA4_MPI-ESM-LR	27.2	12.8	7.9	36.5	31.7	24.0	10.8	33.1	6.8
RCA4_NorESM1-M	31.1	12.9	7.9	31.6	32.4	27.2	11.6	40.0	9.4
REMO2009_CM5A-LR	19.0	32.3	24.2	30.2	24.7	13.3	14.0	36.1	27.7
REMO2009_EC-EARTH	21.9	23.2	28.2	28.6	31.6	25.8	15.2	25.4	29.3
REMO2009_GFDL-ESM2G	14.8	17.2	20.2	27.8	29.3	3.4	10.2	31.3	18.9
REMO2009_HadGEM2-ES	16.1	20.7	29.4	35.2	33.9	6.4	14.3	32.3	27.2
REMO2009_MIROC5	13.6	22.1	26.4	27.4	34.9	8.2	14.2	25.8	24.9
REMO2009_MPI-ESM-LR	18.4	27.0	17.9	28.3	30.0	20.9	14.1	29.4	25.3

extreme events in the quantile–quantile plots means that each return period regression line can be characterized by two parameters including the 1-year return level and SRRP (as defined in Sect. 2.4). The 1-year return level is analogous to the threshold for the extreme events in the extreme value distribution. The SRRP is the scale parameter of the extreme value distribution. It means that if the threshold and scale parameters are known, estimations or extrapolations can be made for a return period larger than the data record length (in years). Therefore, it is important that the RCMs adequately reproduce these parameters because they have physical connotations. Thresholds, if determined for various weather stations across a region (as in this study), characterize the site to site variation in extreme rainfall conditions. The higher the threshold, the higher are the rainfall extremes (or extents of floods in the area). On the other hand, the higher the value of SRRP, the higher the intermittency in extreme rainfalls at a given station.

Figure 8 shows results of comparison of observed and RCM-based quantiles in terms of bias on the parameters characterizing the regression line in quantile–quantile plots. The value for each RCM in Fig. 8 represents the mean of biases from all the rainfall stations. The bias of the largest magnitude in reproducing 1-year quantile was − 72% obtained by HIRHAM5_NorESM1-M. This was followed by − 68% from RACMO22T_EC-EARTH. The top performance was exhibited by CCLM4-8-17_MPI-ESM-LR (− 11%), followed by CCLM4-8-17_HadGEM2-ES (− 15%). With respect to SRRP, the worst performance was obtained from the CCLM4-8-17_MPI-ESM-LR (176%), followed by CCLM4-8-17_HadGEM2-ES (146%). The top performance was yielded by REMO2009_MIROC5 (2%) and REMO2009_GFDL-ESM2G (3.5%). Considering the mean of biases on both 1-year quantile and the SRRP, the top performance was exhibited by REMO2009_MIROC5 (10.3%), REMO2009_GFDL-ESM2G (10.5%), and RCA4_GFDL-ESM2M (13.8%). The worst performance was obtained by CCLM4-8-17_MPI-ESM-LR (82.2%), and RACMO22T_HadGEM2-ES (− 79.2%).

The details of how the RCMs were biased in reproducing quantiles at each rainfall station can be found in Tables S14–S15 of the Supplementary Material M1. For instance, most simulations of the RCMs under-estimated both threshold and scale parameters of the extreme value

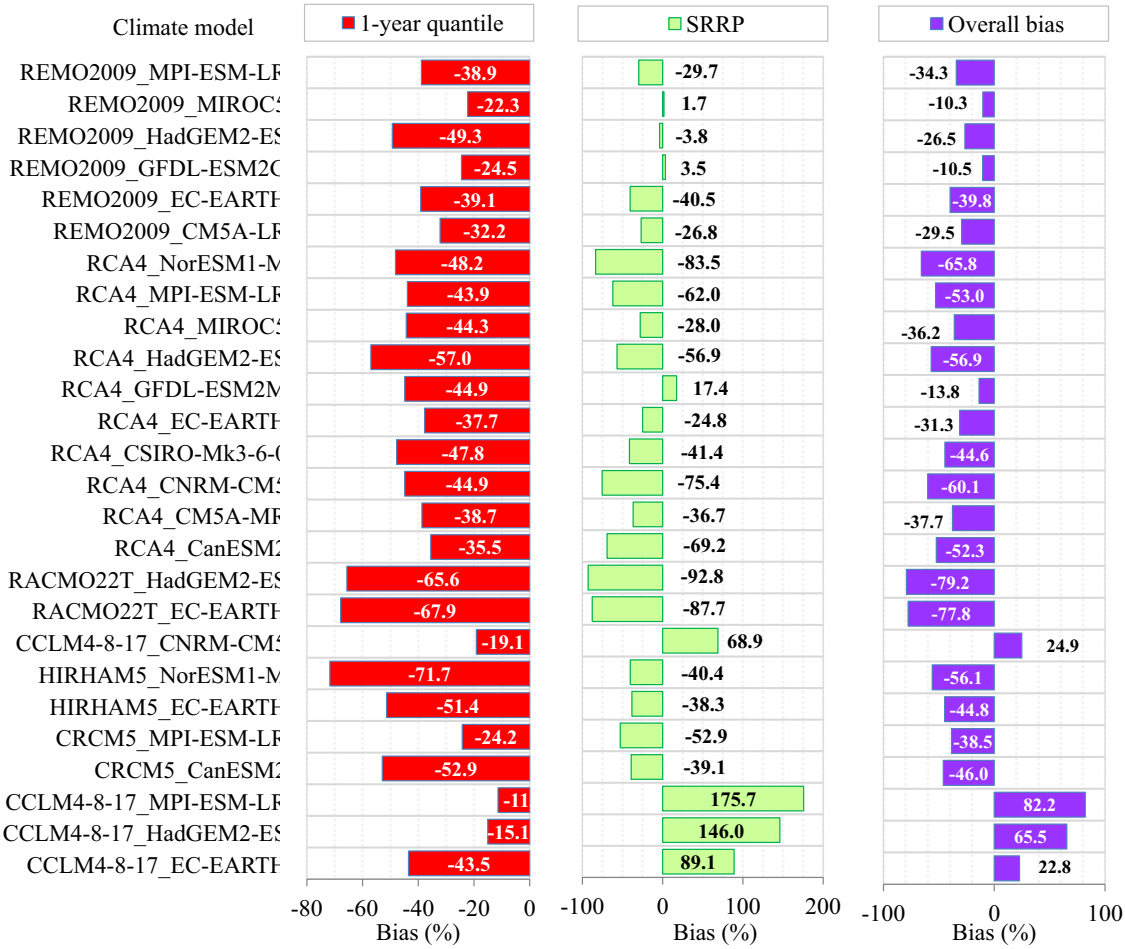

Fig. 8 Bias of RCMs for frequency analysis considering performance at all the selected rainfall stations

distribution (or SRRP). However, at Stations 6–7, and 9, instead most simulations tended to over-estimate the threshold parameter. The ensemble mean of the RCMs' biases for threshold parameter at Stations 1–9 was found to be − 41.2%, − 6.7%, − 15.2%, − 37.5%, − 46.4%, 7.6%, 32.4%, − 47.4%, and 7.8%, respectively. Correspondingly, the ensemble mean of RCMs' biases for reproducing the SRRP was − 16.5%, 64.5%, − 19.1%, − 28.4%, − 11.7%, − 9.8%, − 26.9%, − 42.4%, and 90.1%, respectively. It was more difficult for the RCMs to reproduce the SRRP than the threshold of the extreme rainfall events. Furthermore, the difficulty in reproducing frequency of rainfall extremes varied from one station to another and this was due to the spatial variability in rainfall across the study area.

Figure 9 shows performance of the RCMs with respect to the frequency of rainfall extremes. To obtain Fig. 9, skill score was obtained using data at each of the rainfall stations and the detailed results can be seen from Table S1 of the Supplementary Material M1. Considering all the selected rainfall stations, the top three models in order of their performance to reproduce the threshold parameter of rainfall extremes yielded skill score of 82%, 73%, and 68%, and these were CRCM5_MPI-ESM-LR, CRCM5_CanESM2, and CCLM4-8-17_HadGEM2-ES, respectively. However, with respect to the SRRP, the best (1st, and 2nd) models in order of their of their performance yielded skill score of 80%, and 68%, and these were REMO2009_MIROC5, and REMO2009_MPI-ESM-LR, respectively. The third top performance was obtained by four RCMs including REMO2009_CM5A-LR, REMO2009_EC-EARTH, REMO2009_GFDL-ESM2G, and REMO2009_HadGEM2-ES. Combining performance for both threshold and SRRP parameters, the top three (first, second, and third) RCMs were REMO2009_MIROC5, CRCM5_MPI-ESM-LR, and RCA4_CNRM-CM5, with skill scores of 64%, 61%, and 60%, respectively. To reproduce 1-year quantile, the best performance (with a skill score of 96.2%) at Stations 8 and 9 was exhibited by CRCM5_MPI-ESM-LR. For the remaining Stations 1–7, the highest skill score (96.2%) in 1-year

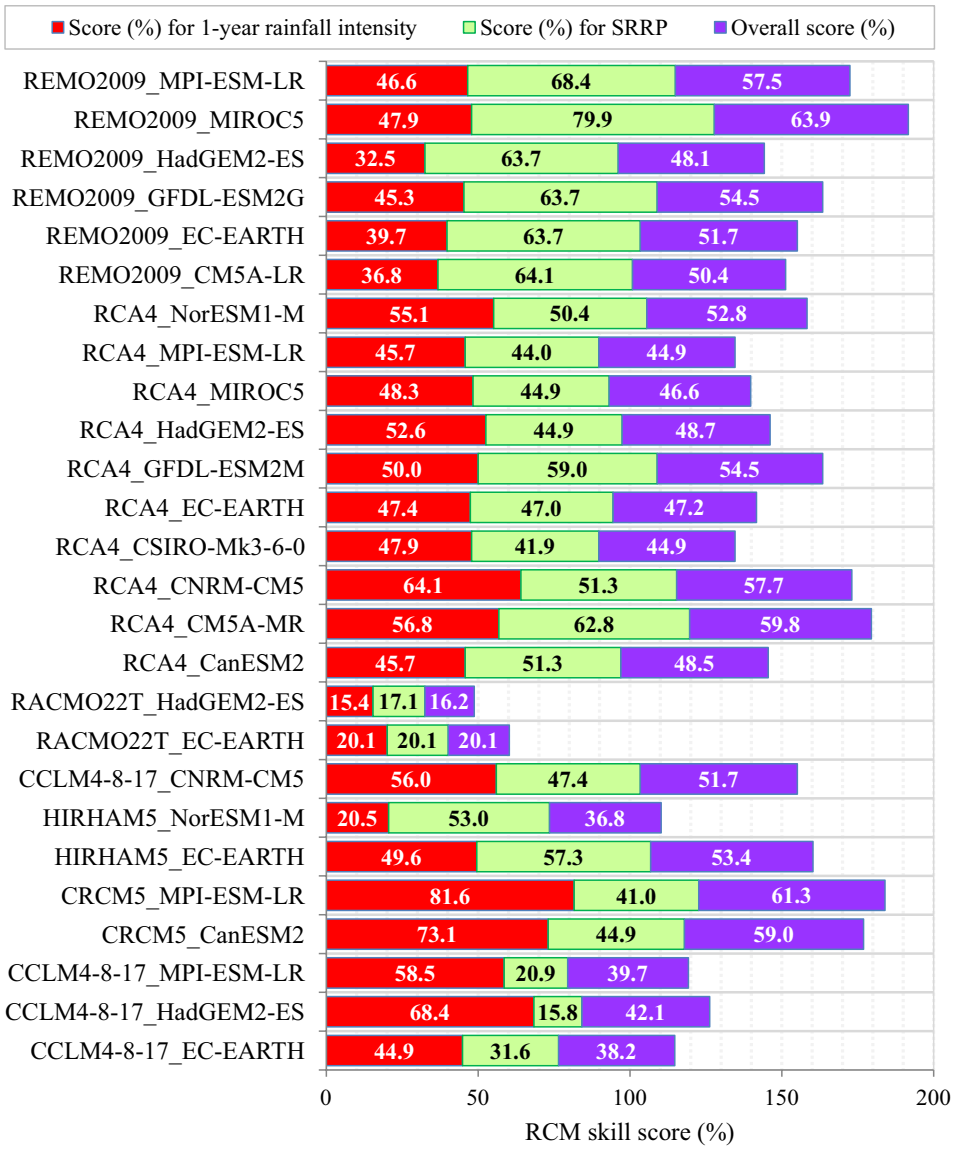

Fig. 9 Skill score of RCMs for frequency analysis considering performance at all the selected rainfall stations

quantile was obtained by CCLM4-8-17_MPI-ESM-LR, CCLM4-8-17_HadGEM2-ES, RCA4_HadGEM2-ES, CCLM4-8-17_EC-EARTH, CCLM4-8-17_CNRM-CM5, RCA4_CNRM-CM5, and REMO2009_HadGEM2-ES, respectively. For reproducing the beta at Stations 1, 6 and 8, the top performing model was REMO2009_MIROC5. However, for Stations 2–4, 5, 7, and 9, the highest skill score was obtained by RCA4_CM5A-MR, REMO2009_GFDL-ESM2G,CCLM4-8-17_CNRM-CM5, REMO2009_CM5A-LR, HIRHAM5_NorESM1-M, and RACMO22T_EC-EARTH, respectively (see Table S1 of the Supplementary Material M1). These results showed that there was not any single simulation which consistently yielded the best results (across the study area) with respect to both threshold and scale parameters. In other words, performance of the CORDEX depended on the selected RCM. It means that the choice of a particular RCM can greatly influence the results from an analysis of extreme rainfall events. To even out such an influence, several simulations of various RCMs are required to be considered for analyses of extreme rainfall events in the context of climate change impact investigations.

3.3 Comparison of CORDEX RCMs and the driving CMIP5 GCMs

Figure 10 shows results for evaluation of RCMs and their driving CMIP5 GCMs in reproducing observed rainfall extremes. The RMSE values for the RCMs and their corresponding driving CMIP5 GCMs in reproducing extreme rainfall conditions at each rainfall station can be found in Tables T13–T18 of the Supplementary Material M2. The

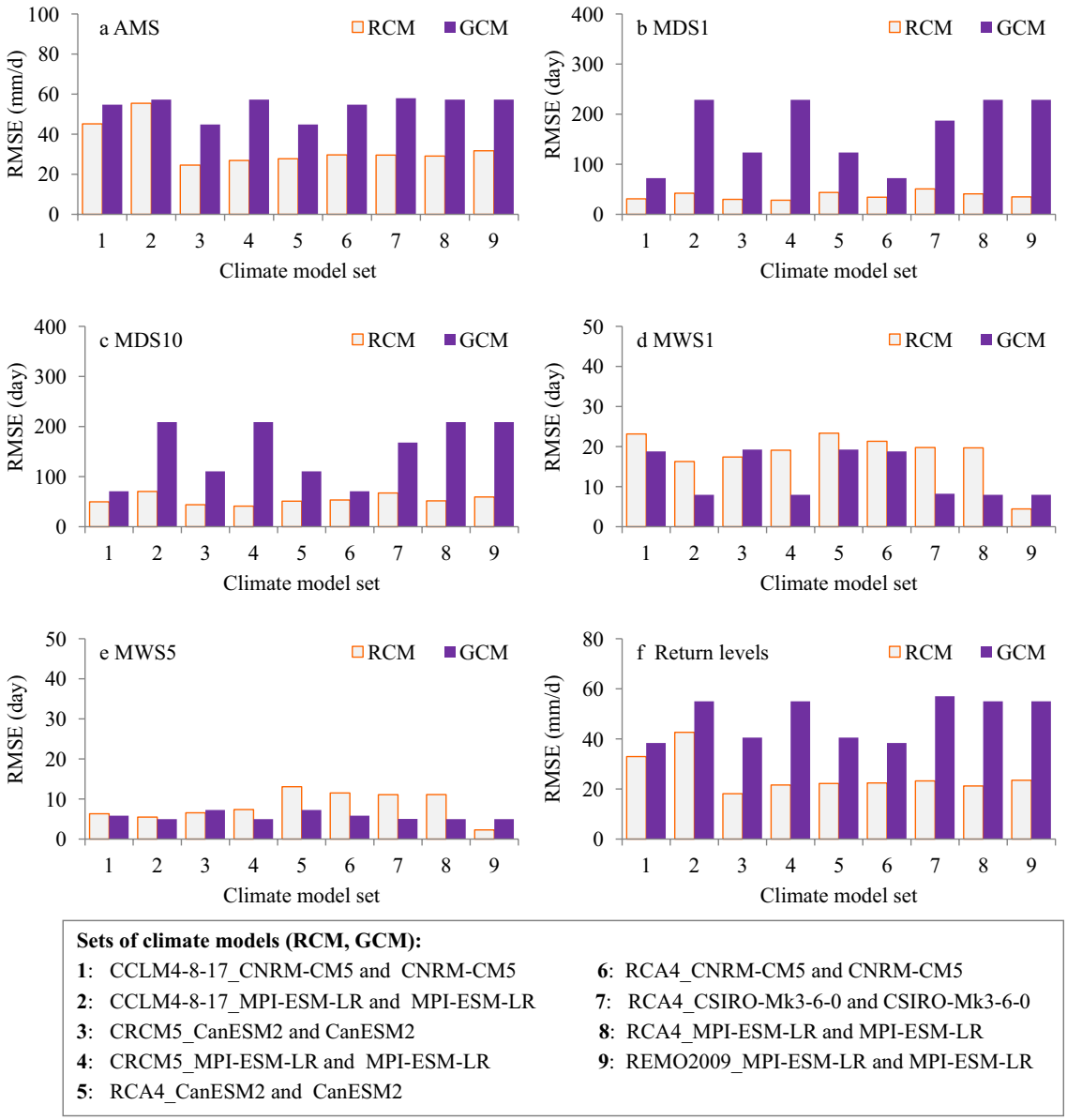

Fig. 10 Comparison of RCMs and their corresponding driving GCMs for reproducing (**a**) AMS, **b**) MDS1, (**c**) MDS10, (**d**) MWS1, (**e**) MWS5, and (**f**) return levels

RMSE values were lower for RCMs than GCMs in reproducing observed AMS, MDS1, MDS10, and frequency of quantiles (Fig. 10a–c, f). However, the RSME values were larger for RCMs than GCMs in simulations of MWS1 and MWS5 (Fig. 10d–e). The smallest difference in RMSE for MDS1, MWS5, and frequency analysis was obtained by climate model set 1 (CCLM4-8-17_CNRM-CM5 and CNRM-CM5). For AMS, MDS10, and MWS1, the smallest differences in the RMSE were produced by climate model sets 2 (CCLM4-8-17_MPI-ESM-LR and MPI-ESM-LR), 6 (RCA4_CNRM-CM5 and CNRM-CM5), and 3 (CRCM5_CanESM2 and CanESM2), respectively. In other words, the difference between the RMSE of RCM and GCM depended on the selected set of climate models. Climate models tend to differ in terms of spatial resolution, and modelled processes, and parameterizations such as cloud physics, and aerosol effects. The CMIP5 GCMs had different spatial resolutions. However, the CORDEX RCMs used in this study had the same spatial resolution.

On average, RMSE of the GCMs (as a percentage of the RMSE of the RCMs) was 70.64% and 68.27% for MSW1, and MWS5, respectively. However, for the simulation of AMS, MDS1, MDS10, and rainfall intensity quantiles, the RCMs' RMSE expressed as percentage of the GCMs'

RMSE yielded 61.70%, 22.51%, 35.72%, and 52.41%, respectively. This showed that in the simulations of dry spells and extreme peak rainfall intensities, the uncertainties in the GCMs were reduced through downscaling by RCMs. However, for reproducing wet conditions (MWS1 and MWS5), the RMSE values of the GCMs were larger than those of the RCMs (except for the climate model set 3). This showed that in the simulation of wet spells, the

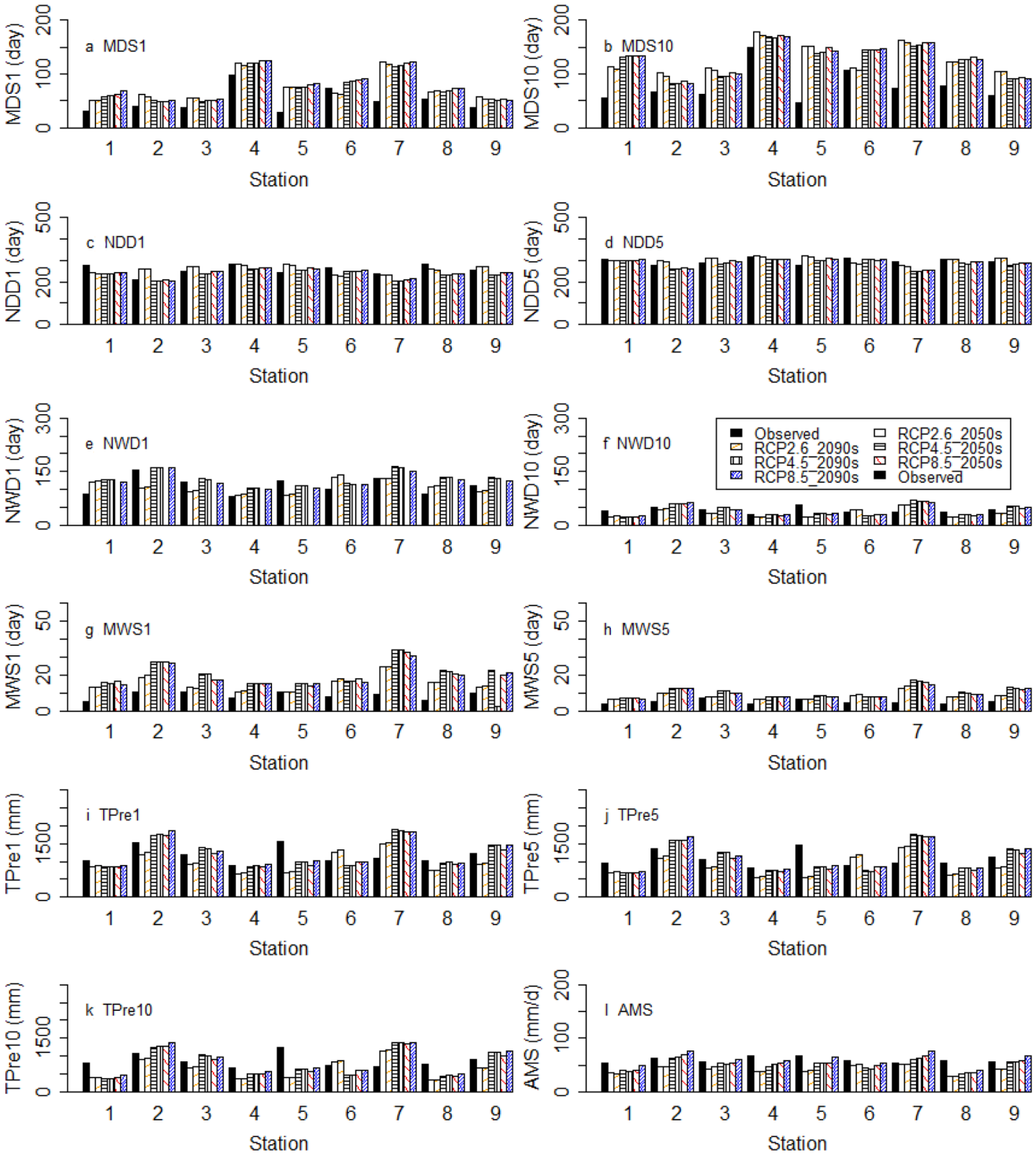

Fig. 11 Observed and ensemble future mean of RCMs' (**a**) MDS1, (**b**) MDS10, (**c**) NDD1, (**d**) NDD5, (**e**) NWD1, (**f**) NWD10, (**g**) MWS1, (**h**) MWS5, (**i**) TPre1, (**j**) TPre5, (**k**) TPre10, (**l**) AMS from observed rainfall and series obtained from the RCMs. All the charts share the same legend as in (**f**)

uncertainties from the GCMs and RCMs possibly added up. Furthermore, climate models exhibited larger uncertainties in the simulation of dry spells than wet spells.

3.4 Changes in rainfall

Figure 11 shows the impacts of climate change on the long-term mean of the ERIs. The maximum consecutive number of dry days in the 2050s and 2090s will generally be larger than those for the past climatic conditions (Fig. 11a–b). The amount by which the dry spells will increase in the future varies from one location to another. For instance, at Stations 2 and 6, the dry spell under RCP4.5 in the 2050s will increase by 25.7% and 14.4%, respectively. Despite the increase in the length of dry spell, the number of dry days in each year is expected to generally reduce across the study area except at Station 5 (Fig. 11c–d). This suggests that the various locations of the study area will become wetter in the future compared with the past period (1961–1990). This can be confirmed by the higher MWS1 and MWS5 for future than past climatic conditions (Fig. 11g–h). Furthermore, the number of wet days at all the selected locations is expected to increase except at Station 5 (Fig. 11e). The inconsistence at Station 5 compared with other locations could be due to the uncertainty from data quality problem. The amount by which the number of wet days is expected to increase depends on the threshold (higher for 1 mm than 10 mm rainfall) (Fig. 11e–f). Based on the rainfall threshold of 10 mm, the number of wet days will increase at Stations 1–3, 7, or 9 and reduce at Stations 5–6 and 8 (Fig. 11f). Compared with the past climatic condition, the future annual total of rainfall will decrease at Stations 1, 4–6, and 8. However, the future rainfall total at Stations 2, 7, and 9 will higher than those of the past condition (Fig. 11i–k). Results of RCP 2.6 showed that the rainfall totals (Fig. 10i–k) and AMS (Fig. 11l) in both the 2050s and 2090s will decrease across the study area. The mean of the maximum rainfall event in each year is expected to increase at Stations 2, 7 and 9 (Fig. 11l). However, the future AMS will be lower than that of the past period at Stations 1, 3, 5–6, and 8. Notably, under the RCP 8.5, the 2090s' AMS at Station 3 will, on average, be slightly higher (by 10.4%) than that of the past period (1961–1990).

Figure 12 shows the amount by which 10-year rainfall quantiles will change in the 2050s and 2090s. The empirical 10-year quantiles at the selected Stations 1–9 over the climate baseline 1961–1990 were 80.6, 91.9, 80.8, 101.3, 106.8, 87.6, 97.8, 108.1, and 82 mm/day, respectively. Based on RCP 2.6, the ranges of the ensemble mean changes (minimum, maximum) are (3.24%, 7.60%) and (4.10%, 9.39%) for the 2050s and 2090s, respectively (Fig. 12a). The amount by which the 10-year quantiles will change under the RCP 4.5 ranges from 4.84% (Station 9) to 17.37% (Station 1) in the 2050s. However, in the 2090s, the changes under the RCP 4.5 will range from 6.16% (Station 9) to 21.03% (Station 1). The ensemble mean changes (minimum, maximum) under the RCP 8.5 are in the ranges

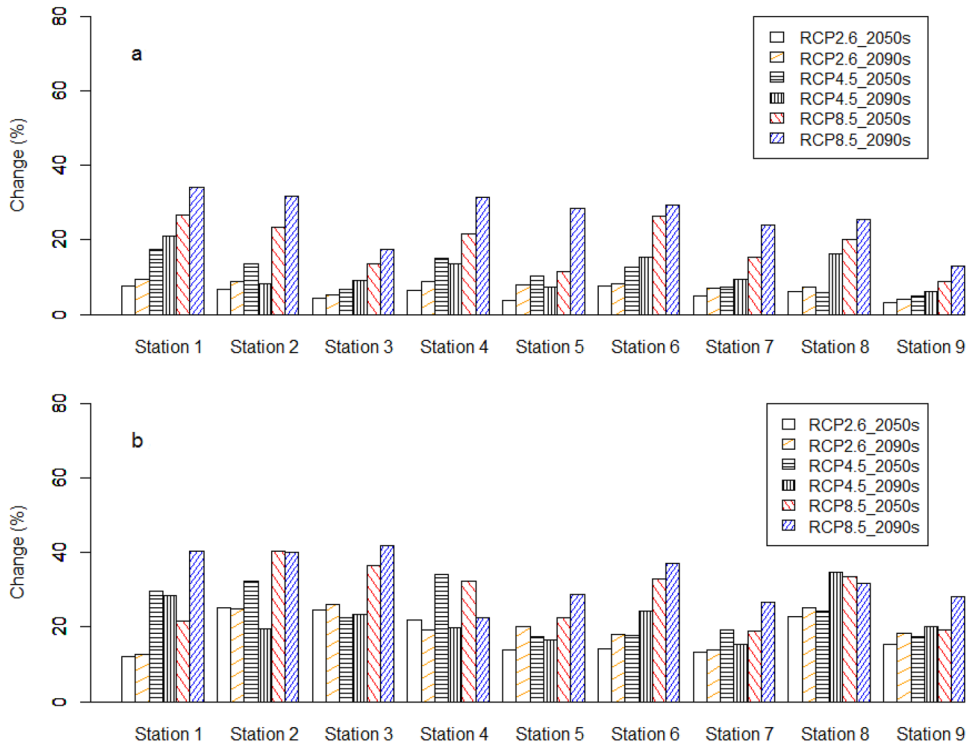

Fig. 12 Ensemble (**a**) mean, and (**b**) standard deviation in projected changes in 10-year return level. Both charts share the same legend as in (**b**)

(8.94%, 26.63%) and (16.42%, 37.54%) for the 2050s and 2090s, respectively (Fig. 12a). A previous study (Onyutha et al. 2016) found that the change in 10-year quantiles across the study area will go up to 43.6% under scenario A2 of the CMIP3. However using the CMIP5, Akurut et al. (2016) showed that rainfall extremes over the Lake Victoria of the LVB will increase by up to about 40%.

At each rainfall station, the amount by which the 10-year quantile will change from the smallest to the largest is for the RCP 2.6, RCP 4.5 and RCP 8.5, respectively. Furthermore, the 10-year rainfall quantiles of the 2090s will be higher than those for the 2050s under all the scenarios. The uncertainties on the projected quantiles were summarized in the form of ensemble standard deviation at each rainfall station (Fig. 12b). For instance, at Station 9, the ensemble standard deviation under RCP 4.5 was 17.5%, and 20.1% in the 2050s and 2090s, respectively. Thus, the RCP4.5 projected changes of 4.84% and 6.16% at this station in the 2050s and 2090s will be in the ranges (− 12.66%, 22.34%), and (− 11.34%, 23.66%), respectively. Such an analysis, for instance, shows the deviations that could be obtained in the design values calculated in a climate change context for planning of water resources applications which depend on return periods of rainfall extremes. The ensemble standard deviations in Fig. 12b fall within 15% and 46%. This range shows differences in the RCMs in projecting the rainfall extremes across the LVB.

4 Discussion and conclusions

To boost confidence in the climate change rainfall projections, it is important that past climatic conditions are adequately reproduced in both space and time by the climate models. This study, using high (or daily) resolution observed rainfall, showed that the CORDEX RCMs largely over- estimated or under-estimated trends and frequency of various rainfall-based climate change indices characterizing the wet and dry conditions across the study area. Performance of each RCM varied from one extreme rainfall index to another. However, observed climate indices were better reproduced by the ensemble means of the RCMs than the individual RCMs thereby confirming the significance considering multi-model ensembles for increasing credibility of climate change projections. Here, the use of multi-model ensembles circumvents the biases of individual RCMs due to the effects of variability. Results also showed that the RCMs reproduced the observed maximum dry spells better than the driving GCMs. For instance, on average, Root Mean Squared Error (RMSE) of the GCMs (as a percentage of the RMSE of the RCMs) was about 70% for reproducing wet spells. The reduction of the GCMs bias for dry spells by RCMs downscaling indicated an improvement in modelling of the processes that control variation and occurrences of dry conditions across the study area. The RMSE values for reproducing wet spells were small or less than 20% for both the RCMs and GCMs. This indicated that the processes responsible for the occurrences and variation of wet spells were reasonably captured by both the RCMs and the their driving GCMs. However, RCMs' RMSE expressed as percentage of the GCMs' RMSE (in reproducing the maximum wet spell) yielded about 30%. Here, the RMSE values of the GCMs were larger than those of the RCMs thereby indicating that the uncertainties from the GCMs and RCMs possibly added up.

Generally, the ensemble mean of the RCMs' biases in simulating trends in each extreme rainfall index was of magnitude above 50%. Ensemble mean biases in reproducing long-term mean were lower than those for trends and frequency of extreme events. Even in the simulation of mean climatic conditions (for instance, seasonal rainfall totals), previous studies (Ayugi et al. 2020; Endris et al. 2013; Kisembe et al. 2018) showed considerable bias or poor performance of several CORDEX RCMs across East Africa. One reason for reduced capacity of the climate models to reproduce past climatic conditions is normally the coarse spatial resolution (especially for the CMIP3 and CMIP5). In this study, the RCMs used were all based on the spatial resolution of 0.44 or 50 km resolution with daily temporal scale as emphasized in the CORDEX framework. The differences in the simulations from the RCMs were not due to resolution but other issues including: (i) how key climatic processes were modelled, and (ii) model parameterization such as cloud physics, and effects of aerosol or Land Use or Land Cover (LULC) changes on rainfall. Question would be why and how the climate models could be possibly improved?

- Changes in LULC can influence exchange of energy and water between land surface and the atmosphere (Pielke et al. 2011). Although not considered before, LULC changes were incorporated (as land forcing data) by the IPCC in the CMPI5 simulations. The RCMs comprise both terrestrial and atmospheric partitions. This makes it possible to employ RCMs and the land surface models to assess land–atmosphere feedback with the context of investigating how the biogeophysical processes through LULC changes can impact on the regional climate. Improvements of the RCMs could be by addressing current challenges such as (i) lack of accurate high resolution descriptions (in both space and time) of land surface covers and characteristics as well as landscape heterogeneity, and (ii) the need for improved representations of urban and non-urban areas. Challenge (i) arises due to the current use of remotely sensed data of coarse spatial resolution to generate land surface descriptions.

- An increase in aerosol loading can potentially reduce (but increase) light (heavy) precipitation and this mainly occurs through the space–time redistribution of precipitation (Alizadeh-Choobari 2018; Fan et al. 2013). Furthermore, aerosol revitalizes the development of deep, thick clouds, but suppresses the formation of low, thin clouds (Liet al.2011). Evidence of the impacts of aerosol on rainfall is well studied (Alizadeh-Choobari 2018; Boo et al. 2015; Ackerley et al. 2011). For instance, the substantial rise in aerosol loading from the European and North American emissions through the changes in North Atlantic Sea Surface Temperatures partially contributed to the 1950–1980 decreasing trend in rainfall across the Sahel (Ackerley et al. 2011; Kawase et al. 2010). It remains possible that the recent rapid increase in the Asian aerosol emissions or the decline in the European and North American emissions may potentially drive the variation in the East African long rains (Rowell et al. 2015). Considerable uncertainty exists when it comes to climate modelling of aerosol impacts. Notably "….the uncertainty in estimates of aerosol radiative forcing still drives an almost threefold uncertainty in total radiative forcing of climate change" (Ghan and Penner 2016). For improved climate models regarding aerosol impacts, missing aerosol components (such as nitrate) should be included, and crudely represented components requires improvement (Ghan and Penner 2016).

It was noted that the RCMs under-estimated rainfall extremes at some locations while in other areas there were over-estimations. To adequately reproduce observed rainfall extremes, the properties or physical processes (ranging from climate dynamics to water droplet formation) of rainfall which vary in both space and time could be considered at a regional scale or even location-based level (if possible). This means regional impacts of natural variability (chaotic nature of the internal components responsible for decadal, multi-decadal, and/or even inter-annual variability) should be well understood and reproduced in climate models. Along the Equator where the study area is located, variation in the band of rainfall which moves along with the Inter-Tropical Convergence Zone (ITCZ) is influenced by regional topographical features including Mountains (Elgon, Rwenzori, Kenya) and Great Lakes (Victoria, Tanganyika, Malawi) (Onyutha et al. 2016). The Great Lakes develop their own circulation through lake breezes (Camberlin 2009). On the other hand, the mountain ranges in the North-eastern part of the LVB (bordering the western Kenyan Highlands) generate their own climate through slope circulation (Okeyo 1987). The enhanced afternoon convection is a reflection of the joint effect of the lake and upslope breezes (Camberlin 2009). The magnitude of the interactive influences from the ITCZ and regional factors vary from location to location across East Africa. For instance, it was shown in a previous study (Onyutha et al. 2016) that the areas in the North-eastern quadrant of the LVB (where Stations 3 and 9) has some June–July–August–September (JJAS) rainfall yet the JJAS is a long dry season for the rest of the areas across the study area. In other words, the long-term (1961–1990) rainfall over other areas containing Stations 1–2, and 4–8 exhibited a bimodal pattern with rainy March–April–May (MAM) and October–November–December (OND). Apart from the ITCZ and regional factors, attention could be geared towards how to adequately represent and eventually model in the RCMs the regional and/or local impacts of global climate phenomenon such as the El Niño Southern Oscillation ENSO the dominant mode of inter-annual climate variability, and Indian Ocean Dipole (IOD). The IOD (or the difference in the Sea Surface Temperature (SST) between the eastern and the western parts of the Indian Ocean) has positive and negative phases which are linked to the variation of wet and dry conditions, respectively, across the study area. The southern boundary of the ITCZ is strongly correlated with the meridional SST gradient events (Freitas et al. 2017). The ITCZ southern boundary has the potential to link the IOD and ENSO; furthermore, very strong ENSO and IOD events can lead to greater than normal shifts in the ITCZ southern boundary (Freitas et al. 2017). Generally, the IOD and ENSO events are closely linked. Actually, only about 32% of IOD events occur independently of ENSO events (Stuecker et al. 2017). This means that a climate model simulating strong IOD events also generates strong ENSO events. However, the IOD–ENSO relationship depends on the selected time scale. The dominant time scales to control the IOD–ENSO relationship are 1.5, 3 and 24 years Sang et al. (2019). "*The overall CMIP5 performance in the IOD simulation does not show remarkable improvements compared to CMIP3*" (Liu et al. 2014). The CMIP5 performed worse than the CMIP3 in reproducing the Bjerknes dynamic air-sea feedback (equatorial zonal wind response to SST anomaly); this was due to the under-estimation of the wind response to SST forcing while over-estimating the thermocline response to surface wind forcing by the CMIP5 models (Liu et al. 2014). Important dynamical and thermo-dynamical feedbacks in the tropical Indian Ocean including the Bjerknes air-sea feedback, ocean subsurface temperature response to the thermocline variations, thermodynamic air–sea coupling that comprises the wind-evaporation-SST, and cloud-radiation-SST feedback, and thermocline response to equatorial zonal wind forcing (Liu et al. 2014) should be adequately reproduced by the CORDEX RCMs if the they are to be driven by the CMIP5 GCMs as the initial and lateral boundary conditions.

Rainfall exhibits strong spatio-temporal variability, as well as fractal behaviour. A process is said to be fractal if it cannot be defined by the classical Euclidian mathematics. While considering various drivers of rainfall, models could

incorporate fractals. In considering climate dynamics, forecasting models which incorporate fractals tend to be appreciably reliable on a regional scale (Rangarajan and Sant 1997). In line with fractals, observations very far away in time can depend on one another, and this feature is important in rainfall prediction. Measures of such dependence can be in terms of the Hurst exponent (Hurst 1951) characterizing the large-scale and/or multiple-scale variability in the series. Periods of, say, 10, 20, and 30 years can show how trends vary in time. If, for instance, a 30-year time frame is considered and analyses of changes conducted over several sub-periods, rising and falling sub-trends can be revealed (Onyutha 2016). These large-scale fluctuations of sub-trends can occur in a random way. Such fluctuations are actually indicative of the Hurst phenomenon something which is related to climate change (Evans 1996). Natural variation in rainfall (in terms of statistical dependence properties such as scaling behaviour) can greatly influence the overall uncertainty in the climate change simulations and/or projections especially of extreme climatic conditions. Statistical dependence can be implemented based on two frameworks. In the Markovian approach, the latest observations are considered to influence the future probabilities. Alternatively in a framework which combines the approach of Kolmogorov (1940) and Hurst (1951), the simulations of rainfall for the future climatic conditions can be conditioned on all the observations from the past period (for instance, from 1900 till present). Characterizing natural variability in terms of statistical dependence through the incorporation of fractals or long-range dependence or the Hurst phenomenon requires long-term observed series of high temporal and spatial resolution for reliably calibrating climate models before prediction of future climatic conditions.

Long-term observed data especially in Africa is lacking and policy makers should heavily invest in weather data collection to support scientific research (Onyutha 2019). This will still take some time into the future to ensure the issue of data limitation and questionable quality is addressed. Given the scarcity of long-term observed data especially in Africa, an option for the use of reanalyses data could be explored. However, prior to their use, reanalyses data need to be bias corrected especially in locations where they are significantly biased. Furthermore, several reanalyses datasets need to be assessed to determine which one performs best in reproducing various aspects of observed climatology including trends and variability as well as frequency of extreme rainfall events. This is because, in a climate change context, rainfall extremes are important for planning operation and management of risk-based water resources applications related to floods and drought. Assessments of reanalyses data could also be performed in an event-based way with respect to certain well-known occurrences in the past climatic conditions. For instance, around 1960, rainfall across the Equatorial region (where this study area is located) exhibited step jump in mean, something which the reanalyses data need to adequately reproduce. Importantly, climate change information to support planning of adaptation measures should be accompanied by uncertainties. In this way, planning and/or adopting a particular climate change impact-oriented adaptation strategy can be based on financial cost–benefit analyses.

This study considered only rainfall extreme indices some of which include the maximum wet spell in each year, the maximum dry spell in each year, the annual counts of wet or dry days, the number of dry days in each year, and the rainfall total above threshold of 1 mm. The AMS comprises the severe rainfall intensities responsible for generating runoff of large magnitudes that can cause flooding. The larger the precipitation intensities in the AMS from a selected location, the more susceptible are the low lying areas of the considered catchment to flooding events. In the context of frequency analyses, the AMS can be used to determine the return periods of the flood-causing precipitation intensities for planning flood plain development, design of hydraulic structures such as sewer and river systems, culverts, and bridges. The remaining rainfall indices are based on thresholds of 1 mm, 5 mm, and 10 mm. Definition of thresholds with respect to various drought categories can be found provided by Onyutha (2017). For meteorological applications, thresholds define rainfall amount (given the potential evapotranspiration) in an area over a particular period. Rainfall totals in terms of TPre1, TPre5, and TPre10 are important for planning and management of crop systems and practices. When considering agricultural drought, threshold can be taken to define the amount of rainfall required to keep the soil moisture at a level which avoids crop failure without any references to surface water resources. Various crops require different amounts of soil moisture (or rainfall thresholds) to avoid their failures (Food and Agriculture Organization FAO 1986). Rainfall total (in terms of TPre1, TPre5, or TPre10) can vary across regions thereby defining which areas are suitable for particular crops. This is important for planning a careful selection of which crop to plant at a location given the rainfall total over a rainy season. Areas with lower than normal rainfall totals require planting of drought-resistant crops. Wet spell (MWS1 and MWS5) and Dry spell (MDS1 and MDS10) are relevant for understanding durational aspects of extreme rainfall conditions. In the context of frequency analyses, MWS and MDS characterize the probabilities of risk related to the occurrences of extreme wet and dry conditions, respectively. The metrics MWS1, MWS5, MDS1 and MDS10 are relevant for planning how to meet crop water requirements, for instance through irrigation schedules. Number of dry (NDD1, NDD5) and wet (NWD1, NWD10) days are important to characterize incidence of dry and wet conditions. Incidence of drought is the ratio of the number of all the days with the rainfall below the

threshold to the total number of days within the period under consideration expressed as percentage (Onyutha 2017). For the incidence of wet conditions, the number of days with rainfall above the stipulated threshold is considered. Generally, incidence expresses the commonness of drought or wet conditions at a place for the given period. This is relevant for planning of reservoir operations.

It was noted that assessment of the performance of RCMs or climate models can be influenced by (i) the choice of the goodness-of-fit measures, and (ii) criteria for extracting the extreme climatic indices. This means that the use of several criteria for evaluating performance of climate models is important for consistence and coherence of research findings. It is envisaged that the capacity of RCMs may depend on the selected climatic variable. Therefore, it is important to evaluate climate models with respect to several climate change indices based on both precipitation and temperature. Some temperature-related indices such as the hottest day and coldest night can be relevant for monitoring human health in a climate changing context.

Finally, the author of this paper wishes to clarify that the findings from this paper were not intended to comprise a negative overall message regarding climate models. However, this study underscores the importance of high quality observed climatic data and the need for continued improvements of climate models to boost confidence in future projections of rainfall extremes across the East African region.

Funding This research did not receive any specific grant from funding agencies in the public, commercial, or not-for-profit sectors.

Compliance with ethical standards

Conflict of interest The author declares that he has no known competing financial interests or personal relationships that could have appeared to influence the work reported in this paper.

References

ACAPS (2018) Uganda: Flooding and landslides in Bududa. Retrieved online via the link https://www.acaps.org/sites/acaps/files/products/files/20181018_acaps_start_briefing_note_uganda_flooding_and_landslides_in_bududa.pdf. Accessed 20 Dec 2019.

Ackerley D, Booth BBB, Knight SHE, Highwood EJ, Frame DJ, Allen MR, Rowell DP (2011) Sensitivity of twentieth-century Sahel rainfall to sulfate aerosol and CO2 forcing. J Clim 24:4999–5014

Ahmadi B, Moradkhani H (2019) Revisiting hydrological drought propagation and recovery considering water quantity and quality. Hydrol Process 33:1492–1505

Ahmadalipour A, Moradkhani H (2018) Escalating heat-stress mortality risk due to global warming in the Middle East and North Africa (MENA). Environ Int 117:215–225

Akurut M, Willems P, Niwagaba CB (2014) Potential impacts of climate change on precipitation over Lake Victoria, East Africa, in the 21st century. Water 6:2634–2659

Alizadeh-Choobari O (2018) Impact of aerosol number concentration on precipitation under different precipitation rates. Meteorol Appl 25:596–605

Anyah RO, Semazzi FHM, Xie L (2006) Simulated physical mechanisms associated with climate variability over Lake Victoria basin in East Africa. Mon Weather Rev 134:3588–3609

Ashouri H, Hsu KL, Sorooshian S, Braithwaite DK, KnappKR CLD, Prat OP (2015) PERSIANN-CDR: daily precipitation climate data record from multisatellite observations for hydrological and climate studies. Bull Am Meteorol Soc 96:69–83

Assefa TA (2016) Analysis of rainfall extremes under climate variability in Upper Blue Nile basin. MSc Dissertation, KU Leuven and Vrije Universiteit Brussel, Belgium.

Ayugi B, Tan G, Gnitou GT, Ojara M, Ongoma V (2020) Historical evaluations and simulations of precipitation over East Africa from Rossby centre regional climate model. Atmos Res 232:104705. https://doi.org/10.1016/j.atmosres.2019.104705

Berhane A, Hadgu G, Worku W, Abrha B (2020) Trends in extreme temperature and rainfall indices in the semi-arid areas of Western Tigray. Ethiopia Environ Syst Res 9(3):1–20. https://doi.org/10.1186/s40068-020-00165-6

Boo K-O, Booth BBB, Byun Y-H, Lee J, Cho CH, Shim SB, Kim K-T (2015) Influence of aerosols in multi-decadal SST variability simulations over the North Pacific. J Geophys Res Atmos 120:517–531

Cattani E, Merino A, Guijarro JA, Levizzani V (2018) East Africa Rainfall trends and variability 1983–2015 using three long-term satellite products. Remote Sens 10(6):931. https://doi.org/10.3390/rs10060931

Climate Home News (2013) Climate change linked to 2011 East Africa drought. Retrieved online via the link https://www.climatechangenews.com/2013/02/21/climate-change-linked-to-2011-east-africa-drought/ Accessed 21 Dec 2019.

EM-DAT (2018) The Emergency Events Database—Université Catholique de Louvain (UCL)—CRED, D. Guha-Sapir. www.emdat.be (Brussels, Belgium retrieved at 23 January 2018).

Endris HS, Omondi P, Jain S, Lennard C, Hewitson B, Chang'a L, Awange JL, Dosio A, Ketiem P, Nikulin G, Panitz HJ, Büchner M, Stordal F, Tazalika L (2013) Assessment of the performance of CORDEX regional climate models in simulating East African rainfall. J Clim 26:8453–8475

Evans TE (1996) The effects of changes in the world hydrological cycle on availability of water resources. In: Bazzaz F, Sombroek W (eds) Global climate change and agricultural production: direct and indirect effects of changing hydrological pedological and plant physiological processes. FAO and Wiley, Chichester

Fan J, Leung LR, Rosenfeld D, Chen Q, Li Z, Zhang J, Yan H (2013) Microphysical effects determine macro physical response for aerosol impacts on deep convective clouds. PNAS 110:E4581–E4590

FAO (1986) Irrigation water management: Irrigation water needs. Rome: food and agriculture organization of the United Nations (FAO). https://www.fao.org/3/S2022E/s2022e00.htm. Accessed 04 April 2020

Floodlist (2016) Ethiopia—20,000 families displaced by floods. https://floodlist.com/africa/ethiopia-families-displaced-belg-rain-floods-may-2016. Accessed 27 Dec 2019.

Floodlist (2019) Ethiopia – Over 20 Killed in Landslide in South. https://floodlist.com/africa/ethiopia-landslide-snnpr-october-2019. Accessed: 22 Dec 2019.

Freitas ACV, Aímola L, Ambrizzi T, de Oliveira CP (2017) Extreme intertropical convergence zone shifts over southern maritime continent. Atmos Sci Let 18:2–10

Funk C, Peterson P, Landsfeld M, Pedreros D, Verdin J, Shukla S, Michaelsen J (2015) The climate hazards infrared precipitation with stations – a new environmental record formonitoring

extremes Sci. Data 2:150066. https://doi.org/10.1038/sdata.2015.66
Ghan S, Penner JE (2016) ARM-Led improvements in aerosols in climate and climate models. Meteorol Monogr 27(5):1–12. https://doi.org/10.1175/AMSMONOGRAPHS-D-15-0033.1
Gebrechorkos SH, Hülsmann S, Bernhofer C (2019) Changes in temperature and precipitation extremes in Ethiopia, Kenya, and Tanzania. Int J Climatol 39:18–30
Gumbel EJ (1958) Statistics of Extremes. Columbia University Press, New York
Haile GG, Tang Q, Sun S, Huang Z, Zhang X, Liu X (2019) Droughts in East Africa: Causes, impacts and resilience. Earth Sci Rev 193:146–161
Harrison L, Funk C, Peterson P (2019) Identifying changing precipitation extremes in Sub-Saharan Africa with gauge and satellite products. Environ Res Lett 14(085007):1–12. https://doi.org/10.1088/1748-9326/ab2cae
Huffman GJ, Bolvin DT, Nelkin EJ, Wolff DB, Adler RF, Gu G, Hong Y, Bowman KP, Stocker EF (2007) The TRMM Multisatellite precipitation analysis (TMPA): quasi global, multiyear, combined-sensor precipitation estimates at fine scales. J Hydrometeorol 8:38–55
Hurst HE (1951) Long-term storage capacity of reservoirs. Trans Am Soc Civil Eng 116:770–799
IPCC (2013) The physical science basis. contribution of working group I to the fifth assessment report of the intergovernmental panel on climate change. In: Stocker TF, Qin D, Plattner G-K, Tignor M, Allen SK, Boschung J, Nauels A, Xia Y, Bex V, Midgley PM (eds). Cambridge University Press, Cambridge, United Kingdom and New York, NY, USA, pp 1535.
Jarvis A, Reuter HI, Nelson A, Guevara E (2008) Hole-filled seamless SRTM data V4, International Centre for Tropical Agriculture (CIAT) https://srtm.csi.cgiar.org. Accessed 20th Dec 2019
Jenkinson AF (1955) The frequency distribution of the annual maximum (or minimum) of meteorological elements. Q J Roy Meteor Soc 81:158–171
Kawase H, Abe M, Yamada Y, Takemura T, Yokohata T, Nozawa T (2010) Physical mechanism of long-term drying trend over tropical North Africa. Geophys Res Lett 37:L09706. https://doi.org/10.1029/2010GL043038
Kendall MG (1975) Rank correlation methods, 4th edn. Charles Griffin, London
Kisembe J, Favre A, Dosio A, Lennard L, Sabiiti G, Nimusiima A (2018) Evaluation of rainfall simulations over Uganda in CORDEX regional climate models. Theor Appl Climatol 137(1–2):1117–1134
Kolmogorov AN (1940) Wienersche Spiralen und Einige Andere Interessante Kurven in Hilbertschen Raum. Doklady Akademii nauk URSS 26:115–118
Li Z, Niu F, Fan J, Liu Y, Rosenfeld D, Ding Y (2011) Long-term impacts of aerosols on the vertical development of clouds and precipitation. Nature Geosci 4:888–894
Liu L, Xie S-P, Zheng X-T, Li T, Du Y, Huang G, Yu W-D (2014) Indian Ocean variability in the CMIP5 multi-model ensemble: the zonal dipole mode. Clim Dyn 43:1715–1730
Mann HB (1945) Nonparametric tests against trend. Econometrica 13(3):245–259
Nashwan MS, Shahid S (2019) Spatial distribution of unidirectional trends in climate and weather extremes in Nile river basin. Theo Appl Climatol 137:1181–1199
Novella NS, Thiaw WM (2013) African rainfall climatology version 2 for famine early warning systems. J Appl Meteorol Climatol 52:588–606
Muthoni FK, Odongo VO, Ochieng J, Mugalavai EM, Mourice SK, Hoesche-Zeledon I, Mwila M, Bekunda M (2019) Long-term spatial-temporal trends and variability of rainfall over Eastern and Southern Africa. Theo Appl Climatol 137:1869–1882
Nikulin G, Jones C, Giorgi F, Asrar G, Büchner M, Cerezo-Mota R, Christensen OB, Déqué M, Fernandez J, Hänsler A, Meijgaard EV, Samuelsson P, Sylla MB, Sushama L (2012) Precipitation climatology in an ensemble of CORDEX-Africa regional climate simulations. J Clim 25:6057–6078
Okeyo AE (1987) The influence of lake Victoria on the convective activities over the Kenya highlands. J Meteorol Soc Japan 65:689–695
Onyutha C, Willems P (2015) Uncertainty in calibrating generalised Pareto distribution to rainfall extremes in Lake Victoria basin. Hydrol Res 46(3):356–376
Onyutha C (2019) African food insecurity in a changing climate: the roles of science and policy. Food Energy Sec 8(1):e00160. https://doi.org/10.1002/fes3.160
Onyutha C (2017) On rigorous drought assessment using daily time scale: Non-stationary frequency analyses, revisited concepts, and a new method to yield non-parametric indices. Hydrology 4:48. https://doi.org/10.3390/hydrology4040048
Onyutha C (2016) Identification of sub-trends from hydro-meteorological series. Stoch Environ Res Risk Assess 30:189–205
Onyutha C, Tabari H, Rutkowska A, Nyeko-Ogiramoi P, Willems P (2016) Comparison of different statistical downscaling methods for climate change rainfall projections over the Lake Victoria basin considering CMIP3 and CMIP5. J Hydro-Environ Res 12:31–45
Pickands J (1975) Statistical inference using extreme order statistics. Ann Stat 3(1):119–131
Pielke RA, Pitman A, Niyogi D, Mahmood R, McAlpine C, Hossain F, Goldewijk KK, Nair U, Betts R, Fall S, Reichstein M, Kabat P, de Noblet N (2011) Land use/land cover changes and climate: modeling analysis and observational evidence. Wiley Interdiscip Rev Clim Chang 2(6):828–850
Rangarajan G, Sant DA (1997) A climate predictability index and its applications. Geophys Res Lett 24:239–1242
Reliefweb (2019) Several killed as landslides hit Bududa, Sironko. https://reliefweb.int/report/uganda/several-killed-landslides-hit-bududa-sironko. Accessed 20 Dec 2019.
Reuter HI, Nelson A, Jarvis A (2007) An evaluation of void filling interpolation methods for SRTM data. Int J Geogr Inform Sci 21(9):983–1008
Rowell DP, Booth BBB, Nicholson SE, Good P (2015) Reconciling past and future rainfall trends over East Africa. J Clim 28:9768–9788
Sang Y, Singh VP, Xu K (2019) Evolution of IOD-ENSO relationship at multiple time scales. Theor Appl Climatol 136:1303–1309
Sheffield J, Goteti G, Wood EF (2006) Development of a 50-year high-resolution global dataset of meteorological forcings for land surface modeling. J Clim 19:3088–3111
Stuecker MF, Timmermann A, Jin F-F, Chikamoto Y, Zhang W, Wittenberg AT, Widiasih E, Zhao S (2017) Revisiting ENSO/Indian Ocean Dipole phase relationships. Geophys Res Lett 44(5):2481–2492
Zhang X, Alexander L, Hegerl GC, Jones P, Tank AK, Peterson TC, Trewin B, Francis W, Zwiers FW (2011) Indices for monitoring changes in extremes based on daily temperature and precipitation data. WIREs Clim Change 2:851–870